2

Conceptual Foundations

2.1 Introduction

This chapter presents the conceptual foundations of plasma turbulence theory from the perspective of physical kinetics of quasi particles. It is divided into two sections:

A) Dressed test particle model of fluctuations in a plasma near equilibrium

B) K41 beyond dimensional analysis - revisiting the theory of hydrodynamic turbulence.

The reason for this admittedly schizophrenic beginning is the rather unusual and atypical niche that plasma turbulence occupies in the pantheon of turbulent and chaotic systems. In many ways, most (though not all) cases of plasma turbulence may be thought of as weak turbulence, spatiotemporal chaos, or wave turbulence, as opposed to fully developed turbulence in neutral fluids. Dynamic range is large, but nonlinearity is usually *not* overwhelmingly strong. Frequently, several aspects of the linear dynamics

persist in the turbulent state, though wave breaking is possible, too. While a scale-to-scale transfer is significant, emission and absorption locally, at a particular scale, are not negligible. Scale invariance is usually only approximate, even in the absence of dissipation. Indeed, it is fair to say that plasma turbulence lacks the elements of simplicity, clarity and universality which have attracted many researchers to the study of high Reynolds number fluid turbulence. In contrast to the famous example, plasma turbulence is a problem in the dynamics of a *multi-scale and complex system.* It challenges the researchers to isolate, define and solve interesting and relevant thematic or idealized problems which illuminate the more complex and intractable whole. To this end, then, it is useful to begin by discussing two rather different 'limiting case paradigms', which is some sense 'bound' the position of most plasma turbulence problems in the intellectual realm. These limiting cases are:

- The test particle model (TPM) of a near-equilibrium plasma, for which the relevant quasi-particle is a dressed test particle,
- The Kolmogorov (K41) model of a high Reynolds number fluid, very far from equilibrium, for which the relevant quasi-particle is the fluid eddy.

The TPM illustrates important plasma concepts such as local emission and absorption, screening response and the interaction of waves and sources. The K41 model illustrates important turbulence theory concepts such as scale similarity, cascades, strong energy transfer between scales and turbulent dispersion. We also briefly discuss turbulence in two-dimensions - very relevant to strongly magnetized plasmas - and turbulence in pipe flows. The example of turbulent pipe flow, usually neglected by physicists in deference to homogeneous turbulence in a periodic box, is especially relevant

to plasma confinement, as it constitutes *the* prototypical example of eddy viscosity and mixing length theory, and of profile formation by turbulent transport. The prominent place accorded in engineering texts to this deceptively simple example is no accident - engineering, after all, need answers to real world problems. More fundamentally, just as the Kolmogorov theory is a basic example of self-similarity in scale, the Prandtl mixing length theory nicely illustrates self-similarity in space. The choice of these particular two paradigmatic examples is motivated by the huge disparity in the roles of spectral transfer and energy flux in their respective dynamics. In the TPM, spectral transport is ignorable, so the excitation at each scale k is determined by the local balance of excitation and damping at that scale. In the inertial range of turbulence, local excitation and damping are negligible, and all scales are driven by spectral energy flux - i.e., the cascade - set by the dissipation rate. (See Fig.2.1 for illustration.) These two extremes correspond, respectively, to a state with no flux and a flux-driven state, in some sense 'bracket' most realizations of (laboratory) plasma turbulence, where excitation, damping and transfer are all roughly comparable. For this reason, they stand out as conceptual foundations, and so we begin out study of plasma turbulence with them.

2.2 Dressed Test Particle Model of Fluctuations in a Plasma near Equilibrium

2.2.1 Basic Ideas

Virtually *all* theories of plasma kinetics and plasma turbulence are concerned, in varying degrees, with calculating the fluctuation spectrum and relaxation rate for plasmas under diverse circumstances. The simplest, most

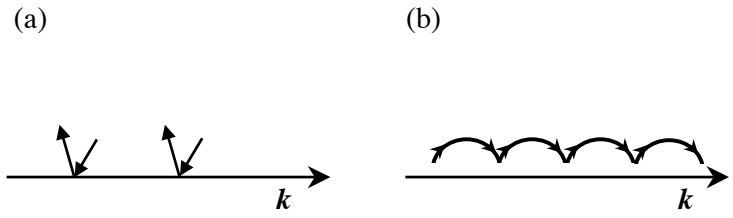

Fig. 2.1. (a)Local in $\boldsymbol{k}$ emission and absorption near equilicrium. (b)Spectral transport from emission at k_1, to absorption at k_2 via nonlinear coupling in a non-equilibrium plasma.

successful and best known theory of plasma kinetics is the *dressed test particle model* of fluctuations and relaxation in a plasma near equilibrium. This model, as presented here, is a synthesis of the pioneering contributions and insights of Rosenbluth, Rostoker, Balescu, Lenard, Klimontovich, Dupree, and others. The unique and attractive feature of the test particle model is that it offers us a physically motivated and appealing picture of dynamics near equilibrium which is *entirely consistent* with Kubo's linear response theory and the fluctuation-dissipation theorem, but does *not* rely upon the abstract symmetry arguments and operator properties which are employed in the more formal presentations of generalized fluctuation theory, as discussed in texts such as Landau and Lifshitz' "Statisical Physics". Thus, *the test particle model is consistent with formal fluctuation theory, but affords the user far greater physical insight.* Though its applicability is limited to the rather simple and seemingly dull case of a stable plasma 'near' thermal equilibrium, the test particle model nevertheless constitutes a vital piece of the conceptual foundation upon which all the more exotic kinetic theories

are built. For this reason we accord it a prominent place it in our study, and begin our journey by discussing it in some depth.

Two questions of definition appear immediately of the outset. These are:

a) What is a plasma?

b) What does 'near-equilibrium' mean?

For our purposes, a plasma is a quasi-neutral gas of charged particles with thermal energy far in excess of electrostatic energy (i.e. $k_{\rm B}T \gg q^2/\bar{r}$), and with many particles within a Debye sphere (i.e. $1/n\lambda_{\rm D}^3 \ll 1$), where q is a charge, $\bar{r}$ is a mean distance between particles, $\bar{r} \sim n^{-1/3}$, n is a mean density, T is a temperature, and $k_{\rm B}$ is the Boltzmann constant. The first property distinguishes a gaseous plasma from a liquid or cristal, while the second allows its description by a Boltzmann equation. Specifically, the condition $1/n\lambda_{\rm D}^3 \ll 1$ means that discrete particle effects are, in some sense, 'small' and so allows truncation of the BBGKY hierarchy at the level of a Boltzmann equation. This is equivalent to stating that if the two body correlation $f(1,2)$ is written in a cluster expansion as $f(1)f(2) + g(1,2)$, then $g(1,2)$ is of $O(1/n\lambda_{\rm D}^3)$ with respect to $f(1)f(2)$, and that higher orders correlations are negligible. Figure 2.2 illustrates a test particle surrounded by many particle in a Debye sphere. The screening on the particle 'A' is induced by other particles. When the particle 'B' is chosen as a test particle, others (including 'A') produce screening on 'B'. Each particle acts the role of test particle and the role of screening for other test particle.

The definition of 'near equilibrium' is more subtle. A near equilibrium plasma is one characterized by:

1) a balance of emission and absorption by particles at a rate related to the temperature, T

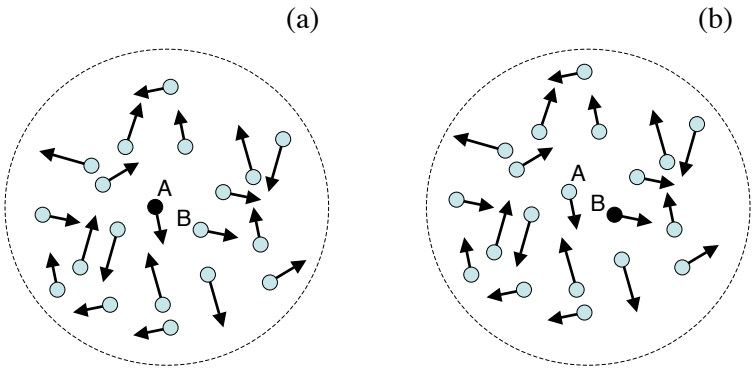

Fig. 2.2. A large number of particles exist within a Debye sphere of particle 'A' (shown by red) in (a). Other particles provide a screening on the particle 'A'. When the particle 'B' is chosen as a test particle, others (including 'A') produce screening on 'B' (b). Each particle acts the role of test particle and the role of screening for other test particle.

2) the viability of linear response theory and the use of linearized particle trajectories.

Condition 1) necessarily implies the absence of linear instability of collective modes, but *does not* preclude collectively enhanced relaxation to states of higher entropy. Thus, a near-equilibrium state need not to be one of maximum entropy. Condition 2) *does* preclude zero frequency convective cells driven by thermal fluctuations via mode-mode coupling, such as those which occur in the case of transport in 2D hydrodynamics. Such low frequency cells are usually associated with long time tails and require a renormalized theory of the non-linear response for their description as is discussed in later chapters.

The essential element of the test particle model is the compelling physical

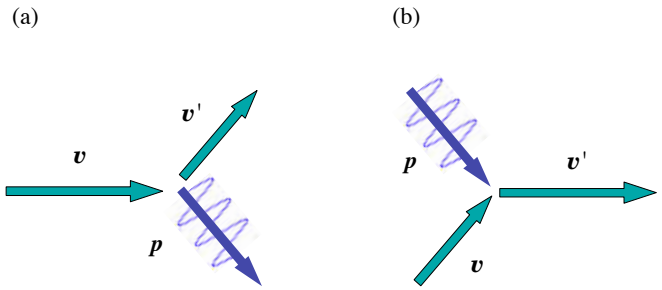

Fig. 2.3. Schematic drawing of the emission of the wave by one particle and the absorption of the wave.

picture it affords us of the balance of emission and absorption which are intrinsic to thermal equilibrium. In the test particle model (TPM), *emission* occurs as a discrete particle (i.e. electron or ion) moves through the plasma, Cerenkov emitting electrostatic waves in the process. This emission process creates *fluctuations* in the plasma and converts particle kinetic energy (i.e. thermal energy) to collective mode energy. Wave radiation also induces a *drag* or dynamical friction on the emitter, just as the emission of waves in the wake of a boat induces a wave drag force on the boat. Proximity to equilibrium implies that emission is, in turn, balanced by *absorption*. Absorption occurs via Landau damping of the emitted plasma waves, and constitutes a wave energy dissipation process which heats the resonant particles in the plasma. Note that this absorption process ultimately returns the energy which was radiated by the particles to the thermal bath. The physics of wave emission and absorption which defines the thermal equilibrium balance intrinsic to the TPM is shown in Fig.2.3.

A distinctive feature of the TPM is that in it, each plasma particle has a

'dual identity', both as an 'emitter' and an 'absorber'. As an emitter, each particle radiates plasma waves, which is moving along some specified, linear, unperturbed orbit. Note that each emitter is identifiable (i.e. as a discrete particle) while moving through the Vlasov fluid, which is composed of other particles. As an absorber, each particle helps to define an element of the Vlasov fluid responding to, and (Landau) damping the emission from, *other* discrete particles. In this role, particle discreteness is smoothed over. Thus, the basic picture of an equilibrium plasma is one of a soup or gas of *dressed test particles*. In this picture, each particle:

i.) stimulates a collective response from the other particles by its discreteness

ii.) responds to on 'dresses' other discrete particles by forming part of the background Vlasov fluid.

Thus, if one views the plasmas as a pea soup, then the TPM is built on the idea that 'each pea in the soup acts like soup for all the other peas'. The *dressed test particle* is the *fundamental quasi-particle* in the description of near-equilibrium plasmas. Examples for dressing by surrounding media are illustrated in Fig.2.4. In a case of a sphere in fluid, the surrounding fluid moves with it, so that the effective mass of the sphere (defined by the ratio between the external force to the acceleration) increases by an amount of $(2\pi/3)\,\rho a^3$, where a is a radius of the sphere and ρ is a mass density of the surrounding fluid. The supersonic object radiates the wake of waves (b), thus its motion deviates from one in vacuum.

At this point, it is instructive to compare the test particle model of thermal equilibrium to the well-known elementary model of Brownian fluctuations

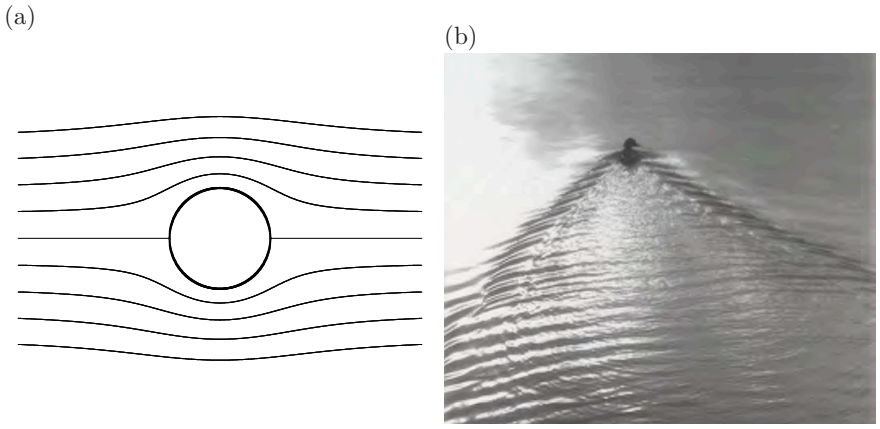

Fig. 2.4. Dressing of moving objects. Examples like a sphere in a fluid (a) and a supersonic object (b) are illustrated. In a case of a sphere, the surrounding fluid moves with it, so that the effective mass of the sphere (measured by the ratio between the acceleration to the external force) increases. The supersonic object radiates the wake of sound wave.

of a particle in a thermally fluctuating fluid. This comparison is given in Table 2.1, below.

Predictably, while there are many similarities between Brownian particle and thermal plasma fluctuations, a key *difference* is that in the case of Brownian motion, the roles of emission and absorption are clearly distinct and played, respectively, by random forces driven by thermal fluctuations in the fluid and by Stokes drag of the fluid on the finite size particle. In contrast, for the plasma the roles of both the emitter and absorber are played by the *plasma particles themselves* in the differing guises of discreteness and as chunks of the Vlasov fluid. In the cases of both the Brownian particle and the plasma, the well-known fluctuation-dissipation theorem of statistical dynamics near equilibrium applies, and relates the fluctuation spectrum to

Table 2.1. *Comparison of Brownian particle motion and plasma fluctuations.*

	Brownian Motion	Equilibrium Plasma
Excitation	$v_\omega \rightarrow$ velocity mode	$E_{k,\omega} \rightarrow$ Langmuir wave mode
Fluctuation spectrum	$\left\langle \tilde{v}^2 \right\rangle_\omega$	$\left\langle E^2 \right\rangle_{\boldsymbol{k},\omega}$
Emission Noise	$\left\langle \tilde{a}^2 \right\rangle_\omega \rightarrow$ random acceleration by thermal fluctuations	$4\pi q\delta(x - x(t)) \rightarrow$ particle discreteness source
Absorption	Stokes drag on particle	$\mathrm{Im}\,\epsilon \rightarrow$Landau damping of collective modes
Governing Equations	$\dfrac{d\tilde{v}}{dt} + \beta\tilde{v} = \tilde{a}$	$\boldsymbol{\nabla}\cdot\boldsymbol{D} = 4\pi q\delta(x - x(t))$

the temperature and the dissipation via the collective mode dissipation, i.e. $\mathrm{Im}\,\epsilon(k,\omega)$, the imaginary part of the collective response function.

2.2.2 Fluctuation spectrum

Having discussed the essential physics of the TPM and having identified the dressed test particle as a the quasi-particle of interest for the dynamics of near equilibrium plasma, we now proceed to calculate the plasma fluctuation spectrum near thermal equilibrium. We also show that this spectrum is that required to satisfy the fluctuation-dissipation theorem (F-DT). Subsequently, we use the spectrum to calculate plasma relaxation.

2.2.2.1 Coherent response and particle discreteness noise

As discussed above, the central tenets of the TPM are that each particle is both a discrete emitter as well as a participant in the screening or dressing cloud of other particles and that the fluctuations are *weak*, so that linear

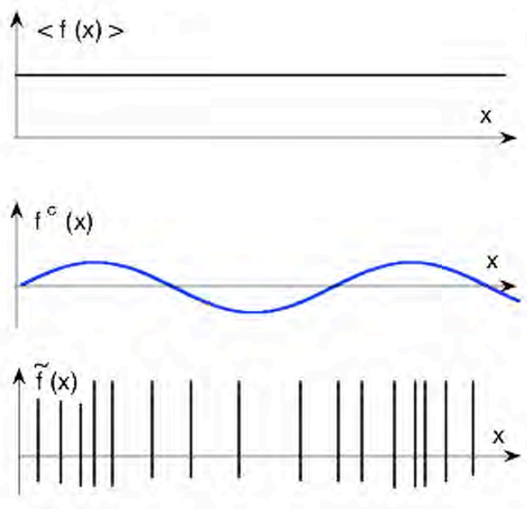

Fig. 2.5. Schematic drawing of the distribution of plasma particles. The distribution function, $f\,(x,v)$, is divided into the mean $\langle f\rangle$, the coherent response $f^{\rm c}$, and the fluctuation part owing to the particle discreteness $\tilde{f}$.

response theory applies. Thus, the total phase space fluctuation δf is written as;

$$\delta f = f^{\rm c} + \tilde{f}, \tag{2.1}$$

where $f^{\rm c}$ is the coherent Vlasov response to an electric field fluctuation, i.e.

$$f^{\rm c}_{k,\omega} = R_{k,\omega} E_{k,\omega},$$

where $R_{k,\omega}$ is a linear response function and $\tilde{f}$ is the particle discreteness noise source, i.e.

$$\tilde{f}(x,v,t) = \frac{1}{n}\sum_{i=1}^{N} \delta(x - x_i(t))\delta(v - v_i(t)) - \langle f\rangle - f^{\rm c} \tag{2.2}$$

(See, Fig.2.5). For simplicity, we consider high frequency fluctuations in an electron-proton plasma, and assume the protons are simply a static background. Consistent with linear response theory, we use unperturbed orbits

to approximate $x_i(t), v_i(t)$ as:

$$v_i(t) = v_i(0) \tag{2.3a}$$

$$x_i(t) = x_i(0) + v_i t. \tag{2.3b}$$

Since $k_{\rm B}T \gg q^2/\bar{r}$, the fundamental ensemble here is one of uncorrelated, discrete test particles. Thus, we can define the ensemble average of a quantity A to be

$$\langle A \rangle = n \int \mathrm{d}\boldsymbol{x}_i \int \mathrm{d}\boldsymbol{v}_i \, f_0(\boldsymbol{v}_i, \boldsymbol{x}_i) \; A \tag{2.4}$$

where $\boldsymbol{x}_i$ and $\boldsymbol{v}_i$ are the phase space coordinates of the particles and f_0 is same near equilibrium distribution, such as a local Maxwellian. For a Vlasov plasma, which obeys

$$\frac{\partial f}{\partial t} + v\frac{\partial f}{\partial x} + \frac{q}{m}E \, \frac{\partial f}{\partial v} = 0 \tag{2.5a}$$

the linear response function $R_{k,\omega}$ is:

$$R_{k,\omega} = -i\frac{q}{m}\frac{\partial \langle f \rangle / \partial v}{\omega - kv}. \tag{2.5b}$$

Self-consistency of the fields and the particle distribution is enforced by Poisson's equation

$$\nabla^2 \phi = -4\pi \sum_{\rm s} n_{\rm s} q_{\rm s} \int \mathrm{d}v \, \delta f_{\rm s} \tag{2.6a}$$

so that the potential fluctuation may be written as

$$\phi_{k,\omega} = -\frac{4\pi n_0 q}{k^2} \int \mathrm{d}v \, \frac{\tilde{f}_{k,\omega}}{\epsilon(k,\omega)}, \tag{2.6b}$$

where the plasma collective response or dielectric function $\epsilon(k,\omega)$ is given by:

$$\epsilon(k,\omega) = 1 + \frac{\omega_p^2}{k} \int \mathrm{d}v \, \frac{\partial \langle f \rangle / \partial v}{\omega - kv}. \tag{2.6c}$$

Note that Eqs.(2.6) relates the fluctuation level to the discreteness noise emission and to $\epsilon(k,\omega)$, the linear collective response function.

2.2.2.2 Fluctuations driven by particle discreteness noise

A heuristic explanation is given here that the 'discreteness' of particles induces fluctuations. Consider a case that charged particles (charge q) are moving as is shown in Fig.2.6(a). Distance between particles is given by d, and particles are moving at the velocity u. (The train of particles in Fig.2.6(a) is a part of distribution of particles. Of course, the net field is calculated by accumulating contributions from all particles.) Charged particles generate the electric field. The time-varying electric field (measured at the position A) is shown in Fig.2.6(b). When we make one particle smaller, but keeping the average density constant, the oscillating field at A becomes smaller. For instance, if the charge of one particle becomes half $q/2$ while the distance between particles becomes half, we see that the amplitude of varying electric field becomes smaller while the frequency becomes higher. This situation is shown in Fig.2.6(b) by a dashed line. In the limit of continuity, i.e.,

Charge per particle $\rightarrow 0$

Distance between particle $\rightarrow 0$,

while the average density is kept constant, the amplitude of fluctuating field goes to zero. This example illustrates why 'discreteness' induces fluctuations.

Before proceeding with calculating the spectrum, we briefly discuss an important assumption we have made concerning collective resonances. For a discrete test particle moving on unperturbed orbits,

$$\tilde{f} \sim q\delta(x - x_{0i}(t))\delta(v - v_i)$$

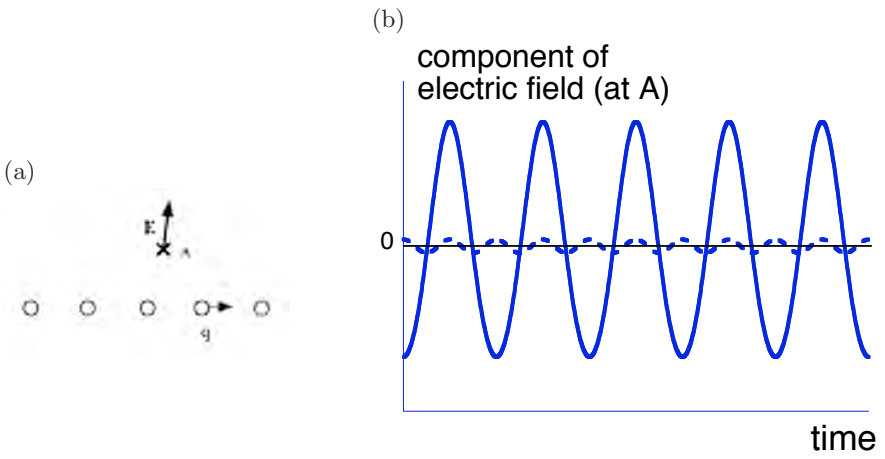

Fig. 2.6. Schematic illustration that the discreetness of particles is the origin of radiations. A train of charged particles (charge q, distance d) are moving near by the observation point A (a). The vertical component of the electric field observed at point A (b). When each particle is divided into two particles, (i.e., charge per particle is $q/2$ and distance between particles is $d/2$), the amplitude of observed field becomes smaller.

so

$$\int \mathrm{d}v\, \tilde{f}_k \sim q e^{-ikvt}$$

and

$$\boldsymbol{\epsilon}(k,t)\phi_k(t) = \frac{4\pi}{k^2} q e^{-ikvt}.$$

Here, the dielectric is written as an operator $\boldsymbol{\epsilon}$, to emphasize the fact that the response is non-local in time, on account of *memory* in the dynamics. Then strictly speaking, we have

$$\phi_k(t) = \boldsymbol{\epsilon}^{-1} \cdot \left[\frac{4\pi q}{k^2} e^{-ikvt} \right] + \phi_{k,\omega_k} e^{-i\omega_k t}. \tag{2.7}$$

In Eq.(2.7), the first term in the RHS is the inhomogeneous solution driven

by discreteness noise, while the second term is the homogeneous solution (i.e. solution of $\boldsymbol{\epsilon}\phi = 0$), which corresponds to an eigenmode of the system (i.e. a fluctuation at k, ω which satisfies $\epsilon(k, \omega) \simeq 0$, so $\omega = \omega_k$). However, the condition that the plasma be 'near equilibrium' requires that all collective modes be damped (i.e. $\mathrm{Im}\,\omega_k < 0$), so the homogeneous solutions decay in time. Thus, in a near equilibrium plasma,

$$\phi_k(t) \xrightarrow[t\to\infty]{} \boldsymbol{\epsilon}^{-1} \cdot \left[\frac{4\pi q}{k^2} e^{-ikvt}\right],$$

so only the inhomogeneous solution survives. Two important caveats are necessary here. First, for weakly damped modes with $\mathrm{Im}\,\omega_{\boldsymbol{k}} \lessapprox 0$, one may need to wait quite a long time indeed to actually arrive at asymptopia, so the homogeneous solutions may be important, in practice. Second, for weakly damped ('soft') modes, the inhomogeneous solution $\hat{\phi} \sim |\mathrm{Im}\,\epsilon|^{-1}$ can become large and produce significant orbit scattering and deflection. The relaxation times of such 'soft modes', thus, increase significantly. This regime of approach to marginality from below is analogous to the approach to criticality in a phase transition, where relaxation times and correlation lengths diverge, and fluctuation levels increase. As in the case of critical phenomena, renormalization is required for an accurate theoretical treatment of this regime. The moral of the story related in this small digression is that the TPM's validity actually fails *prior* to the onset of linear instability, rather than *at* the instability threshold, as is frequently stated. The behavior of fluctuation levels near the stability boundary is schematically illustrated in Fig.2.7. Even if the modes are stable, enhanced excitation of eigenmodes is possible when the controlling parameter is sufficiently close to the boundary of stability, approaching from below. Linear response theory could be violated even if the eigenmodes are stable.

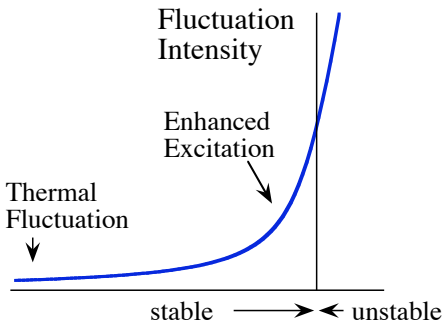

Fig. 2.7. Fluctuation level near the stability boundary. Even if the modes are stable, enhanced excitation of eigenmodes is possible when the controlling parameter approaches the boundary of stability. Linear theory could be violated even if the eigenmodes are stable. Nonlinear noise is no longer negligible.

2.2.2.3 Potential fluctuations

Proceeding with the calculation of the spectrum, we first define the spectral density of the potential fluctuation as the transform of the potential fluctuation correlation function, i.e.

$$\left\langle \phi^2 \right\rangle_{\boldsymbol{k},\omega} = \int_{-\infty}^{\infty} \mathrm{d}\boldsymbol{x} \int_{0}^{\infty} \mathrm{d}t \, e^{i(\omega t - \boldsymbol{k}\cdot\boldsymbol{x})} \left\langle \phi(0,0)\phi(\boldsymbol{x},t) \right\rangle \tag{2.8a}$$

and

$$\left\langle \phi(0,0)\phi(\boldsymbol{x},t) \right\rangle = \int_{-\infty}^{\infty} \frac{\mathrm{d}\boldsymbol{k}}{(2\pi)^3} \int_{-\infty}^{\infty} \frac{\mathrm{d}\omega}{2\pi} e^{i(\boldsymbol{k}\cdot\boldsymbol{x} - \omega t)} \left\langle \phi^2 \right\rangle_{\boldsymbol{k},\omega} . \tag{2.8b}$$

Note that the transformation is a Fourier transform in space but a Laplace transform in time. The "one-sided" Laplace transform is intrinsic to fluctuation and TPM theory, as both are built upon the idea of causality, along with assumptions of stationarity and linear response. As linear response theory applies here, the fluctuation modes are uncorrelated, so

$$\left\langle \phi_{\boldsymbol{k}} \phi_{\boldsymbol{k}'} \right\rangle = (2\pi)^4 \left\langle \phi^2 \right\rangle_{\boldsymbol{k},\omega} \delta(\boldsymbol{k} + \boldsymbol{k}')\delta(\omega + \omega'). \tag{2.8c}$$

Therefore, from Eqs.(2.8a)-(2.8c) and Eq.(2.6b), we can immediately pass to the expression for the potential fluctuation spectrum,

$$\left\langle \phi^2 \right\rangle_{\boldsymbol{k},\omega} = \left(\frac{4\pi n_0}{k^2} q \right)^2 \int \mathrm{d}v_1 \int \mathrm{d}v_2 \, \frac{\left\langle \tilde{f}(1)\tilde{f}(2) \right\rangle_{\boldsymbol{k},\omega}}{|\epsilon(k,\omega)|^2}. \tag{2.9}$$

Note that the fluctuation spectrum is determined entirely by the discreteness correlation function $\left\langle \tilde{f}(1)\tilde{f}(2) \right\rangle$ and the dielectric function $\epsilon(\boldsymbol{k},\omega)$. Moreover, we know ab-initio that since the plasma is in equilibrium at temperature T, the fluctuation-dissipation theorem applies, so that the TPM spectrum calculation *must* recover the general F-DT result, which is;

$$\frac{\left\langle D^2 \right\rangle_{k,\omega}}{4\pi} = \frac{2T}{\omega} \, \mathrm{Im}\, \epsilon(k,\omega). \tag{2.10}$$

Here $\boldsymbol{D}_{k,\omega} = \epsilon(k,\omega)\boldsymbol{E}_{k,\omega}$ is the electric displacement vector. Note that the F-DT quite severely constrains the form of the particle discreteness noise.

2.2.2.4 Correlation of particles and fluctuation spectrum

To calculate $\left\langle \tilde{f}(1)\tilde{f}(2) \right\rangle_{\boldsymbol{k},\omega}$, we must first determine $\left\langle \tilde{f}(1)\tilde{f}(2) \right\rangle$. Since $\tilde{f}$ is the distribution of discrete uncorrelated test particles, we have;

$$\tilde{f}(x,v,t) = \frac{1}{n} \sum_{i=1}^{N} \delta(x - x_i(t))\delta(v - v_i(t)). \tag{2.11}$$

From Eqs. (2.3), (2.4), and (2.11), we obtain

$$\begin{aligned} \left\langle \tilde{f}(1)\tilde{f}(2) \right\rangle = \int \mathrm{d}\boldsymbol{x}_i \int \mathrm{d}\boldsymbol{v}_i \, \frac{\langle f \rangle}{n} \sum_{i,j=1}^{N} [\delta(\boldsymbol{x}_1 - \boldsymbol{x}_i(t)) \\ \times \delta(\boldsymbol{x}_2 - \boldsymbol{x}_j(t))\delta(\boldsymbol{v}_1 - \boldsymbol{v}_i(t))\delta(\boldsymbol{v}_2 - \boldsymbol{v}_j(t))]. \end{aligned} \tag{2.12}$$

Since the product of δ's is non-zero only if the arguments are interchangeable, we obtain immediately the discreteness correlation function

$$\left\langle \tilde{f}(1)\tilde{f}(2) \right\rangle = \frac{\langle f \rangle}{n} \delta(\boldsymbol{x}_1 - \boldsymbol{x}_2)\delta(\boldsymbol{v}_1 - \boldsymbol{v}_2). \tag{2.13}$$

Equation.(2.13) gives the *discreteness correlation function* in *phase space*. Since the physical model is one of an ensemble of discrete, uncorrelated test particles, it is no surprise that $\left\langle \tilde{f}(1)\tilde{f}(2)\right\rangle$ is *singular*, and *vanishes unless the two points in phase space are coincident*. Calculation of the fluctuation spectrum requires the velocity integrated discreteness correlation function $C(\boldsymbol{k},\omega)$ which, using spatial homogeneity, is given by:

$$\begin{aligned} C(\boldsymbol{k},\omega) &= \int \mathrm{d}v_1 \int \mathrm{d}v_2 \left\langle \tilde{f}(1)\tilde{f}(2)\right\rangle_{\boldsymbol{k},\omega} \\ &= \int \mathrm{d}v_1 \int \mathrm{d}v_2 \left[\int_0^\infty \mathrm{d}\tau\, e^{i\omega\tau} \int \mathrm{d}x\, e^{-i\boldsymbol{k}\cdot\boldsymbol{x}} \left\langle \tilde{f}(0)\tilde{f}(\boldsymbol{x},\tau)\right\rangle \right. \\ &\qquad \left. + \int_{-\infty}^0 \mathrm{d}\tau\, e^{-i\omega\tau} \int \mathrm{d}x\, e^{-i\boldsymbol{k}\cdot\boldsymbol{x}} \left\langle \tilde{f}(\boldsymbol{x},-\tau)\tilde{f}(0)\right\rangle \right]. \end{aligned} \tag{2.14}$$

Note that the time history which determines the frequency dependence of $C(\boldsymbol{k},\omega)$ is extracted by propagating particle (2) *forward* in time and particle (1) *backward* in time, resulting in the *two* Laplace transforms in the expression for $C(\boldsymbol{k},\omega)$. The expression for $C(\boldsymbol{k},\omega)$ can be further simplified by replacing v_1, v_2 with $(v_1 \pm v_2)/2$, performing the trivial v-integration, and using unperturbed orbits to obtain

$$\begin{aligned} C(\boldsymbol{k},\omega) &= 2\int \mathrm{d}v \int_0^\infty \mathrm{d}\tau\, e^{i\omega\tau} \int \mathrm{d}x\, e^{-i\boldsymbol{k}\cdot\boldsymbol{x}} \frac{\langle f(v)\rangle}{n} \delta(\boldsymbol{x}-\boldsymbol{v}\tau) \\ &= 2\int \mathrm{d}v\, \frac{\langle f(v)\rangle}{n} \int_0^\infty \mathrm{d}\tau\, e^{i(\omega-\boldsymbol{k}\cdot\boldsymbol{v})\tau} \\ &= \int \mathrm{d}v\, 2\pi \frac{\langle f(v)\rangle}{n} \delta(\omega-\boldsymbol{k}\cdot\boldsymbol{v}). \end{aligned} \tag{2.15}$$

Equation (2.15) gives the well known result for the density fluctuation correlation function in $\boldsymbol{k},\omega$ of an ensemble of discrete, uncorrelated test particles. $C(\boldsymbol{k},\omega)$ is also the particle discreteness noise spectrum. Note that $C(\boldsymbol{k},\omega)$ is composed of the unperturbed orbit propagator $\delta(\omega-\boldsymbol{k}\cdot\boldsymbol{v})$, a weighting function $\langle f\rangle$ giving the distribution of test particle velocities, and the factor of $1/n$, which is a generic measure of discreteness effects. Substitution of

$C(\boldsymbol{k},\omega)$ into Eq.(2.9) then finally yields the explicit general result for the TPM potential fluctuation spectrum:

$$\left\langle \phi^2 \right\rangle_{\boldsymbol{k},\omega} = \left(\frac{4\pi n_0}{k^2} q\right)^2 \frac{\int \mathrm{d}v \, \frac{2\pi}{n} \left\langle f \right\rangle \delta(\omega - \boldsymbol{k}\cdot\boldsymbol{v})}{|\epsilon(\boldsymbol{k},\omega)|^2}. \tag{2.16}$$

2.2.2.5 One-dimensional plasma

In order to elucidate the physics content of the fluctuation spectrum, it is convenient to specialize the discussion to the case of a 1D plasma, for which:

$$C(k,\omega) = \frac{2\pi}{n|k|v_T} F(\omega/k) \tag{2.17a}$$

$$\left\langle \phi^2 \right\rangle_{k,\omega} = n_0 \left(\frac{4\pi q}{k^2}\right)^2 \frac{2\pi}{|k|v_T} \frac{F(\omega/k)}{|\epsilon(k,\omega)|^2}. \tag{2.17b}$$

Here, F refers the average distribution function, with the normalization factor of v_T extracted, $\langle f(v)\rangle = (n/v_T) F(v)$, and v_T is a thermal velocity. It is interesting to observe that $\left\langle \phi^2 \right\rangle_{k,\omega} \sim$ (density) $\times$ (Coulomb spectrum) $\times$ (propagator) $\times$ (particle emission spectrum) $\times$ (screening). Thus, spectral line structure in the TPM is determined by the distribution of Cerenkov emission from the ensemble of discrete particles (set by $\langle f\rangle$) and the collective resonances (where $\epsilon(k,\omega)$ becomes small).

In particular, for the case of an electron plasma with stationary ions, the natural collective mode is the electron plasma wave, with frequency $\omega \simeq \omega_\mathrm{p}(1+\gamma k^2\lambda_\mathrm{D}^2)^{1/2}$ (γ: specific heat ratio of electrons). So for $\omega \gg \omega_\mathrm{p}, kv_T$, $\epsilon \to 1$, we have;

$$\left\langle \phi^2 \right\rangle_{k,\omega} \simeq n_0 \left(\frac{4\pi q}{k^2}\right)^2 \frac{2\pi}{|k|v_T} F(\omega/k), \tag{2.18a}$$

where $F \sim \exp[-\omega^2/k^2v_T^2]$ for a Maxwellian distribution, while in the opposite limit of $\omega \ll \omega_\mathrm{p}, kv_T$ where $\epsilon \to 1 + k^{-2}\lambda_\mathrm{D}^{-2}$, the spectrum becomes

$$\left\langle \phi^2 \right\rangle_{k,\omega} \simeq n_0 (4\pi q)^2 \frac{2\pi}{|k|v_T} \left(1 + 1/k^2\lambda_\mathrm{D}^2\right)^{-2}. \tag{2.18b}$$

In the first, super-celerity limit, the discrete test particle effectively decouples from the collective response, while in the second, quasi-static limit, the spectrum is that of an ensemble of Debye-screened test particles. This region also corresponds to the $k\lambda_{\rm De} \gg 1$ range, where the scales are too small to support collective modes. In the case where collective modes are weakly damped, one can simplify the structure of the screening response via the pole approximation, which is obtained by expanding about ω_k, i.e.

$$\begin{aligned}\epsilon(k,\omega) &= \epsilon_{\rm r}(k,\omega) + i{\rm Im}\,\epsilon(k,\omega) \\ &\simeq \epsilon_{\rm r}(k,\omega_k) + (\omega-\omega_k)\left.\frac{\partial\epsilon}{\partial\omega}\right|_{\omega_k} + i{\rm Im}\,\epsilon(k,\omega_k). \end{aligned} \tag{2.19}$$

So since $\epsilon_{\rm r}(k,\omega_k) \approx 0$,

$$\begin{aligned} 1/|\epsilon|^2 &\simeq \frac{1}{|{\rm Im}\,\epsilon|}\left\{\frac{|{\rm Im}\,\epsilon|}{(\omega-\omega_k)^2|\frac{\partial\epsilon}{\partial\omega}|^2 + |{\rm Im}\,\epsilon|^2}\right\} \\ &\simeq \frac{1}{|{\rm Im}\,\epsilon|\,|\partial\epsilon_{\rm r}/\partial\omega|}\cdot\delta\left(\omega-\omega_k\right). \end{aligned} \tag{2.20}$$

Here it is understood that ${\rm Im}\,\epsilon$ and $\partial\epsilon_{\rm r}/\partial\omega$ are evaluated at ω_k. Notice that in the pole approximation, eigenmode spectral lines are weighted by the dissipation ${\rm Im}\,\epsilon$.

The fluctuation spectrum of plasma oscillations in thermal equailibrium is shown in Fig.2.8. The real frequency and the damping rate of the plasma oscillation are shown as a function of the wavenumber in (a). In the regime of $k\lambda_{\rm De} \ll 1$, the real frequency is close to the plasma frequency, $\omega \sim \omega_{\rm p}$, and the damping rate is exponentially small. The power spectrum of fluctuation as a function of the frequency is illustrated in (b) for various values of the wave number. In the regime of $k\lambda_{\rm De} \ll 1$, a sharp peak appears near the eigenfrequency $\omega \sim \omega_k$. Owing to the very weak damping, the line width is narrow. As the mode number becomes large (in the regime of $k\lambda_{\rm De} \sim 1$), the

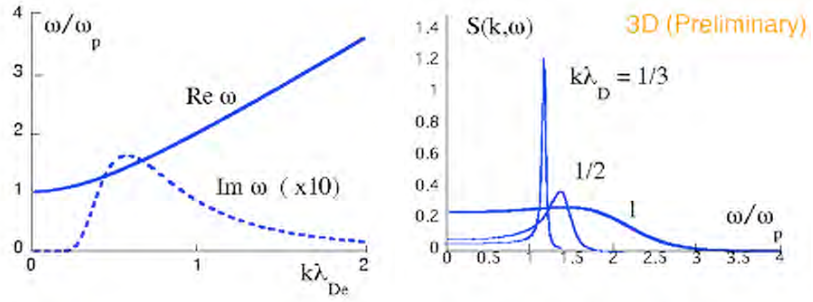

(a) (b)

Fig. 2.8. Illustration of the fluctuation spectrum of plasma oscillations. The real frequency and the damping rate of the plasma oscillation are shown as a function of the wavenumber in (a). In the regime of $k\lambda_{\rm De} \ll 1$, $\omega \sim \omega_{\rm p}$ holds and that the damping rate is exponentially small. The power spectrum of fluctuation as a function of the frequency is illustrated in (b) as a function of the wave number. In the regime of $k\lambda_{\rm De} \ll 1$, a high and sharp peak appears near the eignfrequency $\omega \sim \omega_k$. Owing to the very weak damping, the line width is narrow. As the mode number becomes large an in the regime of $k\lambda_{\rm De} \sim 1$, the bandwidth becomes broader, and the fluctuation intensity becomes high.

bandwidth becomes broader, showing the fact the fluctuations are generated and absorbed very rapidly.

2.2.2.6 Fluctuation-dissipation theorem and energy partition

By now, the reader is surely anxious to see if the results obtained using the test particle model are in fact consistent with the requirements and expectations of generalized fluctuation theory, as advertised. First, we check that Fluctuation-Dissipation Theorem is satisfied. This is most easily ac-

complished for the case of a Maxwellian plasma. There

$$\mathrm{Im}\,\epsilon = -\frac{\omega_\mathrm{p}^2\pi}{k|k|}\frac{\partial\,\langle f\rangle}{\partial v}\bigg|_{\omega/k} = \frac{2\pi\omega}{k^2v_T^2}\frac{\omega_\mathrm{p}^2}{|k|v_T}F_\mathrm{M}(\frac{\omega}{k}), \tag{2.21a}$$

so using Eq.(2.21a) to relate $\mathrm{Im}\,\epsilon(k,\omega)$ to $F(\omega/kv_T)$ in Eq.(2.17b) gives

$$\langle\phi^2\rangle_{k,\omega} = \frac{8\pi T}{k^2\omega}\frac{\mathrm{Im}\,\epsilon}{|\epsilon|^2}, \tag{2.21b}$$

so we finally obtain

$$\frac{\langle D^2\rangle_{k,\omega}}{4\pi} = \frac{2T}{\omega}\mathrm{Im}\,\epsilon \tag{2.21c}$$

is in precise agreement with the statement of the F-DT for a classical, plasma at temperature T. It is important to re-iterate here that applicability of the F-DT rests upon to the applicability of linear response theory for the emission and absorption of each mode. Both fail as the instability marginal point is approached (from below).

Second, we also examine the k-spectrum of energy, with the aim of comparing the TPM prediction to standard expectations for thermal equilibrium, i.e. to see whether energy is distributed according to the conventional wisdom of "$T/2$ per degree-of-freedom" . To this end, it is useful to write (using Eq. (2.21)) the electric field energy as;

$$\frac{|E_{k,\omega}|^2}{8\pi} = \frac{4\pi nq^2}{k|k|}\bigg\{\frac{F(\omega/k)}{(1-\frac{\omega_\mathrm{p}^2}{\omega^2})^2+(\frac{\pi\omega_\mathrm{p}^2}{k|k|}F')^2}\bigg\}, \tag{2.22}$$

where $\epsilon_\mathrm{r} \simeq 1-\omega_\mathrm{p}^2/\omega^2$ for plasma waves, and $F' = \mathrm{d}F/\mathrm{d}u|_{\omega/k}$. The total electric field energy per mode $\mathcal{E}_k$ is given by

$$E_k = \int \mathrm{d}\omega\,|E_{k,\omega}|^2/8\pi, \tag{2.23a}$$

so that use of the pole approximation to the collective resonance and a short calculation then gives

$$E_k = \frac{n_e\omega_\mathrm{p}}{2|k|}\frac{F}{|F'|} = \frac{T}{2}. \tag{2.23b}$$

So, yes – the electric field energy for plasma waves is indeed equipartioned! Since for plasma waves the particle kinetic energy density $E_{\rm kin}$ equals the electric field energy density E_k (i.e. $E_{\rm kin} = E_k$), the total wave energy density per mode W_k is constant at T. Note that Eq. (2.23b) does not imply the divergence of total energy density. Of course, some fluctuation energy is present at very small scales ($k\lambda_{\rm De} \gtrsim 1$) which cannot support collective modes. On such scales, the pole expansion is not valid and simple static screening is a better approximation. A short calculation gives, for $k^2\lambda_{\rm De}^2 > 1,\ E_k \cong (T/2)/k^2\lambda_{\rm De}^2$, so that the *total* electric energy density is

$$\left\langle \frac{E^2}{8\pi} \right\rangle = \int \mathrm{d}k\, E_k$$
$$= \int_{-\infty}^{\infty} \frac{\mathrm{d}k}{2\pi} \frac{T/2}{(1+k^2\lambda_{\rm De}^2)} \sim \left(\frac{nT}{2}\right)\left(\frac{1}{n\lambda_{\rm De}}\right). \qquad (2.24)$$

As Eq. (2.24) is for 1D, there n has the dimensions of particles-per-distance. In 3D, the analogue of this result is

$$\left\langle \frac{E^2}{8\pi} \right\rangle \sim \left(\frac{nT}{2}\right)\left(\frac{1}{n\lambda_{\rm De}^3}\right). \qquad (2.25)$$

so that the total electric field energy equals the total thermal energy times the discreteness factor $1/n\lambda_{\rm De}^3 \sim 1/N$, where N is the number of particles in a Debye sphere. Hence $\left\langle E^2/8\pi \right\rangle \ll nT/2$, as is required for a plasma with weak correlations.

2.2.3 Relaxation Near Equilibrium and the Balescu-Lenard Equation

Having determined the equilibrium fluctuation spectrum using the TPM, we now turn to the question of how to *use it to calculate relaxation near equilibrium*. By "relaxation" we mean the long time evolution of the mean (i.e. ensemble averaged) distribution function $\langle f \rangle$. Here 'long time' means

long or slow evolution in comparison to fluctuation time scales. Generally, we expect the mean field equation for the prototypical example of a 1D electrostatic plasma to have the form of a continuity equation in velocity space, i.e.

$$\frac{\partial \langle f \rangle}{\partial t} = -\frac{\partial}{\partial v} J(v). \tag{2.26}$$

Here, $J(v)$ is a flux or current and $\langle f \rangle$ is the corresponding coarse grained phase space density. $J \xrightarrow[v \to \pm\infty]{} 0$ assures conservation of total $\langle f \rangle$. *The essence of the problem* at hand is *how to actually calculate* $J(v)$! Of course it is clear from the Vlasov equation that $J(v)$ is simply the average acceleration $\langle (q/m) E \delta f \rangle$ due to the phase space density fluctuation δf. Not surprisingly, then, $J(v)$ is most directly calculated using a mean field approach. Specifically, simply substitute the *total* δf into $\langle (q/m) E \delta f \rangle$ to calculate the current $J(v)$. Since $\delta f = f^c + \tilde{f}$, $J(v)$ will necessarily consist of *two* pieces. The *first piece*, $\langle (q/m) E f^c \rangle$, accounts for the *diffusion in velocity* driven by the TPM potential fluctuation spectrum. This contribution can be obtained from a Fokker-Planck calculation using the TPM spectrum as the noise. The *second piece*, $\left\langle (q/m) E \tilde{f} \right\rangle$, accounts for relaxation driven by the *dynamic friction* between the ensemble of discrete test particles and the Vlasov fluid. It accounts for the evolution of $\langle f \rangle$ which must accompany the slowing down of a test particle by wave drag. The second piece has the structure of a drag term. As is shown in the derivation of Eq. (2.16), $\langle E f^c \rangle$ ultimately arises from the discreteness of particles, $\tilde{f}_1$.

The kinetic equation for $\langle f \rangle$ which results from this mean field calculation was first derived by R.Balescu and A. Lenard, and so is named in their honor. The diffusion term of the Balescu-Lenard (B-L) equation is very similar to the quasilinear diffusion operator, discussed in Chapter 3, though

the electric field fluctuation spectrum is prescribed by the TPM and the frequency spectrum is not restricted to eigenmode frequency lines, as in the quasilinear theory. The total phase space current $J(v)$ is similar in structure to that produced by the glancing, small angle Coulomb interactions which the Landau collision integral calculates. However, in contrast to the Landau theory, the B-L equation incorporates *both* static and dynamic screening, and so treats the interaction of collective processes with binary encounters. Screening also eliminates the divergences in the Landau collision integral (i.e. the Coulomb logarithm) which are due to long range electrostatic interactions. Like the Landau integral, the B-L equation is ultimately *nonlinear* in $\langle f \rangle$.

At this point, the skeptical reader will no doubt be entertaining question like "What kind of relaxation is possible here?", "How does it differ from the usual collisional relaxation process?" and "Just what, precisely, does 'near equilibrium' mean?". One point relevant to all these questions is that it is easy to define states which have finite free energy, but which are *stable* to collective modes. One example is the current driven ion acoustic (CDIA) system shown in Fig.2.9. Here the non-zero current, which shifts the electron Maxwellian, constitutes free energy. However, since the shift does not produce a slope in $\langle f_e \rangle$ sufficient to overcome ion Landau damping, the free energy is *not* accessible to linear CDIA instabilities. Nevertheless, electron $\rightarrow$ ion momentum transfer *is* possible, and *can* result in electron relaxation, since the initial state is *not* one of maximum entropy. Here, relaxation occurs via binary interactions of *dressed* test particles. Note however, that in this case relaxation rates may be significantly faster than for 'bare' particle collisions, on account of fluctuation enhancement by weakly damped collec-

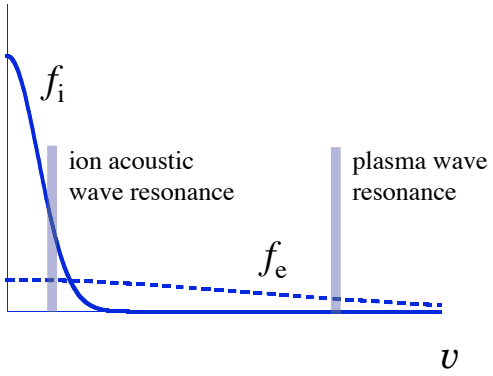

Fig. 2.9. Structure of $\langle f_i \rangle$, $\langle f_e \rangle$ for stable plasma. Velocity space configuration, showing electron plasma wave resonance on the tail of f_e and ion acoustic wave resonance in the bulk of f_e, f_i. In the case with $T_e \gg T_i$, waves can resonate with the bulk of the electron distribution while avoiding ion Landau damping. The slope of f_e is small at resonance, so ion acoustic waves are only weakly damped. In the case with $T_e \sim T_i$, ion acoustic waves resonant in the bulk of f_e cannot avoid ion Landau damping, so the collective modes are heavily damped.

tive modes. Thus, the B-L theory offers both something old and something new relative to its collisional antecedent, the Landau theory.

In order to best elucidate the physics of relaxation processes, we keep the calculations as simple as possible and divide our discussion into three parts. The basic theory is developed for an electrostatic plasma in one dimension, and then applied to single species and two species relaxation processes. Single species relaxation in 3D is then considered followed by a discussion of collective enhancement of momentum exchange.

2.2.3.1 Kinetic equation for mean distribution function

The Balescu-Lenard equation may be derived by a mean-field calculation of the fluctuation-induced acceleration $(q/m)\langle E\delta f\rangle$. Specifically,

$$\begin{aligned}\frac{\partial \langle f\rangle}{\partial t} &= -\frac{\partial}{\partial v}\frac{q}{m}\langle E\delta f\rangle \\ &= -\frac{\partial}{\partial v}J(v)\end{aligned} \tag{2.27}$$

where $J(v)$ must be calculated using the *total* δf, which includes both the linear response f^{c} and the discreteness fluctuation $\tilde{f}$. Thus, substitution of

$$\delta f = f^{\mathrm{c}} + \tilde{f},$$

yields

$$\begin{aligned}J(v) &= -\left(\frac{q}{m}\langle Ef^{\mathrm{c}}\rangle + \frac{q}{m}\left\langle E\tilde{f}\right\rangle\right) \\ &= -D(v)\frac{\partial \langle f\rangle}{\partial v} + F_r(v)\end{aligned} \tag{2.28}$$

where $D(v)$ is the fluctuation-induced diffusion, while $F_r(v)$ is the dynamical friction term. Consistent with linear response theory, we can then write:

$$f^{\mathrm{c}}_{k,\omega} = -i\frac{(q/m)E_{k,\omega}}{\omega - kv}\frac{\partial \langle f\rangle}{\partial v}. \tag{2.29a}$$

so for stationary fluctuations, a short calculation gives:

$$D(v) = \sum_{k,\omega}\frac{q^2}{m^2}k^2\left\langle\phi^2\right\rangle_{k,\omega}\pi\delta(\omega - kv). \tag{2.29b}$$

The spectrum $\left\langle\phi^2\right\rangle_{k,\omega}$ is understood to be the test particle model spectrum, i.e. that of Eq. (2.17b). Similarly, the dynamical friction term $F_r(v)$ is given by

$$F_r(v) = -\frac{q}{m}\sum_{k,\omega} ik\left\langle\phi\tilde{f}\right\rangle_{k,\omega}, \tag{2.30a}$$

where, via Eq. (2.6b), we have:

$$\left\langle \phi\tilde{f} \right\rangle_{k,\omega} = \frac{4\pi n_0 q}{k^2} \int \mathrm{d}v \, \frac{\left\langle \tilde{f}\tilde{f} \right\rangle_{k,\omega}}{\epsilon(k,\omega)^*}. \tag{2.30b}$$

This result explains that the discreteness of particles are the source of correlations in the excited mode. Since

$$\left\langle \phi^2 \right\rangle_{k,\omega} = \left(\frac{4\pi n_0 q}{k^2} \right)^2 \frac{C(k,\omega)}{|\epsilon(k,\omega)|^2},$$

and (from Eq. (2.14))

$$C(k,\omega) = \left\langle \tilde{n}^2 \right\rangle_{k,\omega} = \int \mathrm{d}v \, 2\pi\delta(\omega - kv) \left\langle f(v) \right\rangle,$$

we have

$$\left\langle \phi\tilde{f} \right\rangle_{k,\omega} = \left(\frac{4\pi n_0 q}{k^2} \right) \frac{2\pi\delta(\omega - kv) \left\langle f \right\rangle}{n_0 |\epsilon(k,\omega)|^2}.$$

Thus, the current $J(v)$ is given by;

$$\begin{aligned} J(v) &= -D(v)\frac{\partial \left\langle f \right\rangle}{\partial v} + F_r(v) \\ &= -\sum_{k,\omega} \left(\frac{4\pi n_0 q}{k^2} \right) \frac{q}{m} \left(\frac{2\pi\delta(\omega - kv)}{n_0 |\epsilon(k,\omega)|^2} \right) k \\ &\quad \times \left\{ \left(\frac{4\pi n_0 q}{k^2} \right) \frac{\pi k}{|k| v_T} \left(\frac{q}{m} \right) F(\frac{\omega}{k}) \frac{\partial \left\langle f \right\rangle}{\partial v} + \mathrm{Im}\, \epsilon(k,\omega) \left\langle f \right\rangle \right\}. \end{aligned} \tag{2.31}$$

Note that the contributions from the diffusion $D(v)$ and dynamical friction $F_r(v)$ have been grouped together within the brackets. Poisson's equation relates $\epsilon(k,\omega)$ to the electron and ion susceptibilities $\chi(k,\omega)$ by

$$\epsilon(k,\omega) = \left(1 + \frac{4\pi n_0 q}{k^2} \right) \Big[\chi_i(k,\omega) - \chi_e(k,\omega) \Big],$$

where $\chi_i,\ \chi_e$ are the ion and electron susceptibilities defined by

$$n_{k,\omega} = \chi_i(k,\omega)\phi_{k,\omega}.$$

It is straightforward to show that

$$\mathrm{Im}\, \epsilon(k,\omega) = -\frac{\pi\omega_{\mathrm{p}}^2}{k^2} \frac{k}{|k| v_T} F'(\omega/k) + \mathrm{Im}\, \epsilon_i(k,\omega), \tag{2.32a}$$

where

$$\mathrm{Im}\,\epsilon_i(k,\omega) = \frac{4\pi n_0 q}{k^2}\mathrm{Im}\,\chi_i(k,\omega). \tag{2.32b}$$

Here $\epsilon_i(k,\omega)$ is the *ion* contribution to the dielectric function. Thus, we finally obtain a simplified expression for $J(v)$, which is

$$J(v) = -\sum_{k,\omega}\left(\frac{\omega_\mathrm{p}^2}{k^2}\right)^2\left(\frac{2\pi^2}{n_0 k v_T}\right)\frac{\delta(\omega-kv)}{|\epsilon(k,\omega)|^2} \times\left\{F\left(\frac{\omega}{k}\right)\frac{\partial\langle f\rangle}{\partial v} - \langle f(v)\rangle F'\left(\frac{\omega}{k}\right) + \mathrm{Im}\,\epsilon_i(k,\omega)\langle f\rangle\right\}. \tag{2.33}$$

Equation (2.33) gives the *general* form of the velocity space electron current in the B-L equation for electron relaxation, as described within the framework of the TPM.

In order to elucidate the physics content of $J(v)$, it is instructive to rewrite Eq. (2.33) in alternate forms. One way is to define the fluctuation phase velocity by $u = \omega/k$, so that

$$J(v) = -\sum_{k,\omega}\left(\frac{\omega_\mathrm{p}^2}{k^2}\right)^2\left(\frac{2\pi^2}{n_0 k v_T}\right)\frac{\delta(u-v)}{|k||\epsilon(k,\omega)|^2} \times\left\{F(u)\langle f(v)\rangle' - F'(u)\langle f(v)\rangle + \mathrm{Im}\,\epsilon_i(k,\omega)\langle f(v)\rangle\right\}. \tag{2.34}$$

Alternatively, one could just perform the summation over frequency to obtain

$$J(v) = -\sum_{k}\left(\frac{\omega_\mathrm{p}^2}{k^2}\right)^2\left(\frac{\pi}{n_0 k v_T}\right)\frac{1}{|\epsilon(k,kv)|^2} \times\left\{F(v)\frac{\partial\langle f(v)\rangle}{\partial v} - \langle f(v)\rangle F'(v) + \mathrm{Im}\,\epsilon_i(k,kv)\langle f(v)\rangle\right\}. \tag{2.35}$$

Finally, it is also useful to remind the reader of the counterpart of Eq.(2.33) in the unscreened Landau collision theory, which we write for 3D as:

$$J_\alpha(\boldsymbol{p}) = -\sum_{e,i}\int_{q_\alpha}\mathrm{d}^3q\int\mathrm{d}^3p'\,W(\boldsymbol{p},\boldsymbol{p}',\boldsymbol{q})q_\alpha q_\beta\left\{f(\boldsymbol{p}')\frac{\partial f(\boldsymbol{p})}{\partial \boldsymbol{p}_\beta} - \frac{\partial f(\boldsymbol{p}')}{\partial \boldsymbol{p}'_\beta}f(\boldsymbol{p})\right\}. \tag{2.36}$$

In Eq.(2.36), $W(\boldsymbol{p}, \boldsymbol{p}', \boldsymbol{q})$ is the transition probability for a collision (with momentum transfer $\boldsymbol{q}$) between a 'test particle' of momentum $\boldsymbol{p}$ and a 'field particle' of momentum $\boldsymbol{p}'$. Here the condition $|\boldsymbol{q}| \ll |\boldsymbol{p}|, |\boldsymbol{p}|'$ applies, since long range Coulomb collisions are 'glancing'.

2.2.3.2 Offset on Landau-Rosenbluth Theory

Several features of $J(v)$ are readily apparent. First, just as in the case of the Landau theory, the current $J(v)$ can be written as a sum of electron-electron and electron-ion scattering terms, i.e.

$$J(v) = -\left[D_{e,e}(v)\frac{\partial \langle f \rangle}{\partial v} + F_{e,e}(v) + F_{e,i}(v)\right]. \tag{2.37}$$

Here $D_{e,e}(v)$ refers to the diffusion (in velocity) of electrons by fluctuations excited by electron discreteness emission, $F_{e,e}(v)$ is the dynamical friction on electrons due to fluctuations generated by discreteness, while $F_{e,i}$ is the electron-ion friction produced by the coupling of emission (again due to electron discreteness) to dissipative ion absorption. Interestingly, in 1D,

$$-D_{e,e}(v)\frac{\partial \langle f \rangle}{\partial v} + F_{e,e}(v) \sim \delta(u-v)\{-F(u)\langle f \rangle' + F' \langle f \rangle\} = 0,$$

since $F = \langle f \rangle$ for single species interaction. Thus, we see that *electron - electron friction exactly cancels electron diffusion in 1D*. In this case,

$$J(v) \sim \delta(u-v)\mathrm{Im}\,\epsilon_i(k,\omega)\langle f_e(v) \rangle$$

so that electron relaxation is determined *solely* by electron-ion friction. This result is easily understood from consideration of the analogy between same-species interaction in a stable, 1D plasma and like-particle collisions in 1D (Fig.2.10). On account of conservation of energy and momentum, it is trivial to show that such collisions leave final state = initial state, so no entropy production is possible and no relaxation can occur. This fact is manifested in

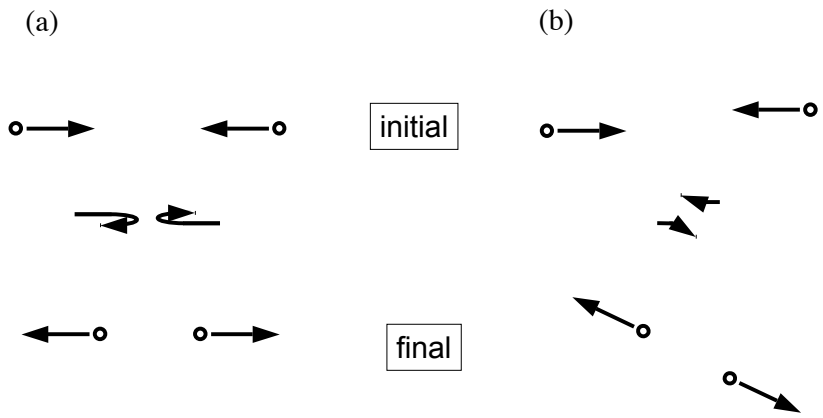

Fig. 2.10. Like-Particle collisions in (a)1D and (b)3D.

the B-L theory by the cancellation between electron - electron terms - since the only way to produce finite momentum transfer in 1D is via inter-species collisions, the only term which survives in $J(v)$ is $F_{e,i}(v)$. Note that this result is not a purely academic consideration, since a strong magnetic field $\boldsymbol{B}_0$ often imposes a 1D structure on the wave -particle resonance interaction in more complicated problems.

A detail comparison and contrast between the Landau theory of collisions and the B-L theory of near-equilibrium relaxation is presented in Table 2.2.

2.2.3.3 Resistivity (Relaxation in one-dimensional system)

Having derived the expression for $J(v)$, it can then be used to calculate transport coefficients and to macroscopically characterize relaxation. As an example, we consider the effective resistivity associated with the current driven system of Fig.2.9. To constract an effective Ohm's Law for this

Table 2.2. *Comparison of Landau and Balescu-Lenard relaxation theory*

	Laudau Theory	B-L Theory
Physical scenario	'test' particle scattered by distribution of 'field' particles	test particle scattered by distribution of fluctuations with $v_{\rm ph} = \omega/k$, produced via discreteness
Scatterer distribution	$f(p')$ field particles distribution	$F(u), \quad u = \omega/k$ fluctuation phase velocity distribution
Correlation	uncorrelated particles as assumed molecular chaos, $\langle f(1,2)\rangle = \langle f(1)\rangle \langle f(2)\rangle$	discrete uncorrelated test particles, $\left\langle \tilde{f}\tilde{f}\right\rangle = (\langle f\rangle/n)\delta(x_-)\delta(v_-)$
Screening	none - Coulomb $\ln\Lambda$ factor put in 'by intuition'	$1/\lvert\epsilon(k,\omega)\rvert^2$
Scattering strength	$\lvert\boldsymbol{q}\rvert \ll \lvert\boldsymbol{p}\rvert$ weak deflection	linear response and unperturbed orbits
Interaction Selection Rule	$W(\boldsymbol{p},\boldsymbol{p}',\boldsymbol{q}) = \delta(p-p')$ in 1D, 1 species	$\delta(u-v)$ in 1D $\delta(\boldsymbol{k}\cdot(\boldsymbol{v}-\boldsymbol{v}'))$ in 3D

system, we simply write

$$\frac{\partial \langle f\rangle}{\partial t} + \frac{q}{m}E_0 \frac{\partial \langle f\rangle}{\partial v} = -\frac{\partial J(v)}{\partial v}, \tag{2.38a}$$

and then multiply by $n_0 q v$ and integrate to obtain, in the stationary limit,

$$\begin{aligned} E_0 &= -\frac{4\pi n_0 q}{\omega_{\rm p}^2}\int {\rm d}v\, J(v) \\ &= 4\pi n_0 |q| \sum_{k,\omega} \frac{\omega_{\rm p}^2}{(k^2)^2}\frac{(2\pi/|k|)}{n_0 k v_T}\left(\frac{{\rm Im}\,\epsilon_i(k,\omega)}{|\epsilon(k,\omega)|^2}\right)\left\langle f_e\left(\frac{\omega}{k}\right)\right\rangle \\ &\equiv \eta_{\rm eff} J_0. \end{aligned} \tag{2.38b}$$

Not surprisingly, the response of $\langle f_e\rangle$ to E_0 cannot unambiguously be written as a simple, constant effective resistivity, since the resonance factor $\delta(\omega -$

kv) and the k, ω dependence of the TPM fluctuation spectrum conflate the field particle distribution function with the spectral structure. However, the necessary dependence of the effective resistivity on electron-ion interaction *is* readily apparent from the factor of $\mathrm{Im}\,\epsilon_i(k,\omega)$. In practice, a non-trivial effect here requires a finite but not excessively strong overlap of electron and ion distributions. Note also that collective enhancement of relaxation below the linear instability threshold *is* possible, should $\mathrm{Im}\,\epsilon(k,\omega)$ become small.

2.2.3.4 Relaxation in three-dimensional system

Having discussed the 1D case at some length, we now turn to relaxation in 3D. The principal effect of three dimensionality is to relax the tight link between particle velocity $\boldsymbol{v}$ and fluctuation phase velocity $(\omega/|k|)\hat{k}$. Alternatively put, conservation constraints on like-particle collisions in 1D force the final state = initial state, but in 3D, glancing collisions which conserve energy and the magnitude of momentum $|\boldsymbol{p}|$, but change the particle's directions, are possible. The contrast between 1D and 3D is illustrated in Fig.2.10. In 3D, the discreteness correlation function is

$$C(k,\omega) = \langle \tilde{n}\tilde{n} \rangle_{k,\omega} = \int \mathrm{d}^3\, v \frac{2\pi}{n_0} \delta(\omega - \boldsymbol{k}\cdot\boldsymbol{v}) \langle f \rangle \,. \tag{2.39}$$

So the B-L current $\boldsymbol{J}(\boldsymbol{v})$ for like particle interactions becomes:

$$\begin{aligned} \boldsymbol{J}(\boldsymbol{v}) = -\sum_{\mathbf{k},\omega} \left(\frac{\omega_\mathrm{p}^2}{k^2}\right)^2 & \frac{2\pi^2 \delta(\omega - \boldsymbol{k}\cdot\boldsymbol{v})}{v_T n_0 |\epsilon(k,\omega)|^2} \\ & \times \boldsymbol{k}\Bigg\{ \int \mathrm{d}\boldsymbol{v}'\, \delta(\omega - \boldsymbol{k}\cdot\boldsymbol{v}') \left\langle f(\boldsymbol{v}') \right\rangle \boldsymbol{k}\cdot \frac{\partial \langle f \rangle}{\partial \boldsymbol{v}} \\ & - \int \mathrm{d}\boldsymbol{v}'\, \delta(\omega - \boldsymbol{k}\cdot\boldsymbol{v}') \boldsymbol{k}\cdot \frac{\partial \langle f \rangle}{\partial \boldsymbol{v}'} \left\langle f(\boldsymbol{v}) \right\rangle \Bigg\}. \end{aligned} \tag{2.40a}$$

Note that the product of delta functions can be re-written as

$$\delta(\omega - \boldsymbol{k}\cdot\boldsymbol{v})\delta(\omega - \boldsymbol{k}\cdot\boldsymbol{v}') = \delta(\omega - \boldsymbol{k}\cdot\boldsymbol{v})\delta(\boldsymbol{k}\cdot\boldsymbol{v} - \boldsymbol{k}\cdot\boldsymbol{v}').$$

We thus obtain an alternate form for $\boldsymbol{J}(\boldsymbol{v})$, which is

$$\boldsymbol{J}(\boldsymbol{v}) = -\sum_{\mathbf{k},\omega}\left(\frac{\omega_{\mathrm{p}}^2}{k^2}\right)^2 \frac{2\pi^2\delta(\omega-\boldsymbol{k}\cdot\boldsymbol{v})}{v_T n_0|\epsilon(k,\omega)|^2} \times\left\{\boldsymbol{k}\int \mathrm{d}\boldsymbol{v}'\,\delta(\boldsymbol{k}\cdot\boldsymbol{v}-\boldsymbol{k}\cdot\boldsymbol{v}')\left[\left\langle f(\boldsymbol{v}')\right\rangle \boldsymbol{k}\cdot\frac{\partial\left\langle f\right\rangle}{\partial\boldsymbol{v}} - \boldsymbol{k}\cdot\frac{\partial\left\langle f\right\rangle}{\partial\boldsymbol{v}'}\left\langle f(\boldsymbol{v})\right\rangle\right]\right\}. \tag{2.40b}$$

This form illustrates an essential aspect of 3D, which is that *only the parallel (to $\boldsymbol{k}$) components of test and field particle velocities* $\boldsymbol{v}$ and $\boldsymbol{v}'$ *need be equal for interaction to occur*. This is in distinct contrast to the case of 1D, where *identity*, i.e. $v = v' = u$, is required for interaction. Thus, relaxation by like-particle interaction is possible, and calculations of transport coefficients are possible, following the usual procedures of the Landau theory.

2.2.3.5 Dynamic Screening

We now come to our final topic in B-L theory, which is *dynamic screening*. It is instructive and enlightening to develop this topic from a direction slightly different than that taken by our discussion up till now. In particular, we will proceed from the Landau theory, but will calculate momentum transfer *including* screening effects and thereby arrive at a B-L equation.

2.2.3.6 Relaxation in Landau model

Starting from Eq. (2.36), the Landau theory expression for the collision-induced current (in velocity) may be written as

$$\boldsymbol{J}_\alpha(\boldsymbol{p}) = \sum_{\text{species}}\int \mathrm{d}^3p'\left[f(\boldsymbol{p})\frac{\partial f(\boldsymbol{p}')}{\partial\boldsymbol{p}'_\beta} - f(\boldsymbol{p}')\frac{\partial f(\boldsymbol{p})}{\partial\boldsymbol{p}_\beta}\right]B_{\alpha,\beta}, \tag{2.41a}$$

where

$$B_{\alpha,\beta} = \frac{1}{2}\int \mathrm{d}\sigma\, q_\alpha q_\beta|\boldsymbol{v}-\boldsymbol{v}'|. \tag{2.41b}$$

The notation here is standard: $d\sigma$ is the differential cross section and $\boldsymbol{q}$ is the momentum transfer in the collision. We will calculate $B_{\alpha,\beta}$ directly, using the some physics assumptions as in the TPM. A background or 'field' particle with velocity $\boldsymbol{v}'$, and charge e' produces a potential field

$$\phi_{k,\omega} = \frac{4\pi e'}{k^2\epsilon(k,\omega)} 2\pi\delta(\omega - \boldsymbol{k}\cdot\boldsymbol{v}'), \tag{2.42a}$$

so converting the time transform gives

$$\phi_{\boldsymbol{k}}(t) = \frac{4\pi e'}{k^2\epsilon(\boldsymbol{k},\boldsymbol{k}\cdot\boldsymbol{v}')} e^{-i\boldsymbol{k}\cdot\boldsymbol{v}'t}. \tag{2.42b}$$

From this, it is straightforward to calculate the net deflection or momentum transfer $\boldsymbol{q}$ by calculating the impulse delivered to a test particle with charge e moving along an unperturbed trajectory of velocity $\boldsymbol{v}$. This impulse is:

$$\boldsymbol{q} = -\int_{\boldsymbol{r}=\boldsymbol{\rho}+\boldsymbol{v}t} \frac{\partial V}{\partial r}\mathrm{d}t, \tag{2.43a}$$

where the potential energy V is just

$$\begin{aligned} V &= e\phi \\ &= 4\pi e e' \int \mathrm{d}^3k \, \frac{e^{i\boldsymbol{k}\cdot\boldsymbol{r}} e^{-i\boldsymbol{k}\cdot\boldsymbol{v}'t}}{k^2\epsilon(\boldsymbol{k},\boldsymbol{k}\cdot\boldsymbol{v}')}. \end{aligned} \tag{2.43b}$$

Here $\boldsymbol{\rho}$ is the impact parameter for the collision, a cartoon of which is sketched in Fig. 2.11. A short calculation then gives the net momentum transfer $\boldsymbol{q}$,

$$\begin{aligned} \boldsymbol{q} &= 4\pi e e' \int \frac{\mathrm{d}^3k}{(2\pi^3)} \, \frac{-i\boldsymbol{k}e^{i\boldsymbol{k}\cdot\boldsymbol{\rho}}\; 2\pi\delta(\boldsymbol{k}\cdot(\boldsymbol{v}-\boldsymbol{v}'))}{k^2\epsilon(\boldsymbol{k},\boldsymbol{k}\cdot\boldsymbol{v}')} \\ &= 4\pi e e' \int \frac{\mathrm{d}^2k_\perp}{(2\pi^3)} \frac{-ik_\perp e^{i\boldsymbol{k}_\perp\cdot\boldsymbol{\rho}}}{k^2\epsilon(\boldsymbol{k},\boldsymbol{k}\cdot\boldsymbol{v}')|\boldsymbol{v}-\boldsymbol{v}'|}. \end{aligned} \tag{2.44}$$

To obtain Eq. (2.44), we used

$$\delta(\boldsymbol{k}\cdot(\boldsymbol{v}-\boldsymbol{v}')) = \frac{\delta(k_\parallel)}{|\boldsymbol{v}-\boldsymbol{v}'|},$$

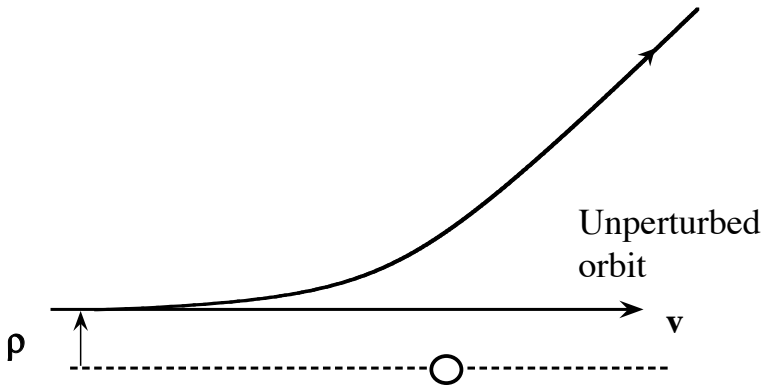

Fig. 2.11. Deflection orbit and unperturbed orbit

and the directions $\parallel$ and $\perp$ are defined relative to the direction of $\boldsymbol{v} - \boldsymbol{v}'$ Since $J \sim \rho^2$, we may write $B_{\alpha,\beta}$ as

$$B_{\alpha,\beta} = \int \mathrm{d}^2\rho \, q_\alpha q_\beta |\boldsymbol{v} - \boldsymbol{v}'|. \tag{2.45}$$

Noting that the $\mathrm{d}^2\rho$ integration just produces a factor of $(2\pi)^2\delta(\boldsymbol{k}_\perp + \boldsymbol{k}'_\perp)$, we can then immediately perform one of the $\int \mathrm{d}^2\boldsymbol{k}_\perp$ integrals in $B_{\alpha,\beta}$ to get

$$B_{\alpha,\beta} = 2e^2e'^2 \int \mathrm{d}^2\boldsymbol{k}_\perp \, \frac{k_{\perp\alpha}k_{\perp\beta}}{|k_\perp^2 \epsilon(\boldsymbol{k}, \boldsymbol{k}\cdot\boldsymbol{v}')|^2 |\boldsymbol{v} - \boldsymbol{v}'|}. \tag{2.46}$$

It is easy to see that Eq.(2.46) for $B_{\alpha,\beta}$ (along with Eq.(2.41a)) is entirely equivalent to the B-L theory for $\boldsymbol{J}(\boldsymbol{v})$. In particular, note the presence of the dynamic screening factor $\epsilon(\boldsymbol{k}, \boldsymbol{k}\cdot\boldsymbol{v}')$. If screening is neglected, $\epsilon \to 1$ and

$$B_{\alpha,\beta} \sim \int \mathrm{d}^2k_\perp \, \frac{k_\perp^2}{|\epsilon| k_\perp^4} \sim \int \mathrm{d}k_\perp / k_\perp \sim \ln(k_{\perp\max}/k_{\perp\min})$$

which is the familiar Coulomb logarithmfrom the Landau theory. Note that

if $\mathbf{k}, \omega \to 0$,

$$k_\perp^2 \epsilon \sim k_\perp^2 + 1/\lambda_{\rm D}^2$$

so that Debye screening eliminates the long range, divergence (associated with $k_{\perp \rm min}$) without the need for an ad-hoc factor. To make the final step toward recovering the explicit B-L result, one can 'un-do' the $\mathrm{d}k_\parallel$ integration and the frequency integration to find

$$B_{\alpha,\beta} = 2(ee')^2 \int_{-\infty}^{\infty} \mathrm{d}\omega \int_{k<k_{\rm max}} \mathrm{d}^3k\, \delta(\omega - \boldsymbol{k}\cdot\boldsymbol{v})\delta(\omega - \boldsymbol{k}\cdot\boldsymbol{v'}) \frac{k_\alpha k_\beta}{k^4 |\epsilon(\boldsymbol{k},\omega)|^2}. \quad (2.47)$$

Here $k_{\rm max}$ is set by the distance of closest approach, i.e.

$$k_{\rm max} \sim \frac{\mu v_{\rm rel}^2}{2ee'}.$$

Substituting Eq.(2.47) for $B_{\alpha,\beta}$ into Eq.(2.41a) recovers Eq.(2.40a). This short digression convincingly demonstrates the equivalence of the B-L theory to the Landau theory with dynamic screening.

2.2.3.7 Collective mode

We now explore the enhancement of relaxation by weakly damped collective modes. Consider a stable, two species plasma with electron and ion distribution functions as shown in Fig. 2.9. This plasma has no free energy (i.e. no net current), but is not necessarily a maximum entropy state, if $T_e \neq T_i$. Moreover, the plasma supports two types of collective modes, namely

i.) electron plasma waves, with $v_{Te} < \omega/k$.

ii.) ion acoustic waves, with $v_{Ti} < \omega/k < v_{Te}$,

where v_{Te} and v_{Ti} are the electron and ion thermal speeds, respectively. Electron plasma waves are resonant on the tail of $\langle f_e \rangle$, where there are few particles. Hence plasma waves are unlikely to influence relaxation in a significant way. On the other hand, ion acoustic waves are resonant in

the *bulk* of the elctron distribution. Moreover, if $T_e \gg T_i$, it is easy to identify a band of electron velocities with significant population levels f but for which ion Landau damping is negligible. Waves resonant there will be weakly damped, and so may substantially enhance relaxation of $\langle f_e(v)\rangle$. It is this phenomenon of collectively enhanced relaxation that we seek to explore quantitatively.

To explore collective enhancement of relaxation, we process from Eq.(2.47), make a pole expansion around the ion acoustic wave resonance and note for ion acoustic wave, $\omega < \boldsymbol{k}\cdot\boldsymbol{v}$ (for electrons), so

$$B_{\alpha,\beta} = 2\pi q^4 \int_{-\infty}^{\infty} \mathrm{d}\omega \int \mathrm{d}^3k\, \delta(\boldsymbol{k}\cdot\boldsymbol{v})\delta(\boldsymbol{k}\cdot\boldsymbol{v}')\frac{\delta\epsilon_r(\boldsymbol{k},\omega_{\boldsymbol{k}})}{|\mathrm{Im}\,\epsilon(\boldsymbol{k},\omega)|}. \tag{2.48}$$

Here $\epsilon_{\mathrm{r}}(\boldsymbol{k},\omega_{\boldsymbol{k}}) = 0$ for wave resonance, and $e = e' = q$, as scattered and field particles are all electrons. $\mathrm{Im}\,\epsilon(\mathbf{k},\omega)$ refers to the collective mode dissipation rate. Now, changing variables according to

$$\begin{aligned} R &= \boldsymbol{k}\cdot\hat{n}, \\ k_1 &= \boldsymbol{k}\cdot\boldsymbol{v}, \qquad k_2 = \boldsymbol{k}\cdot\boldsymbol{v}' \\ \hat{n} &= \boldsymbol{v}\times\boldsymbol{v}'/|\boldsymbol{v}\times\boldsymbol{v}'|. \end{aligned}$$

We have

$$\mathrm{d}^3k = \mathrm{d}R\mathrm{d}k_1\mathrm{d}k_2/|\boldsymbol{v}\times\boldsymbol{v}'|$$

so the $k_1,\ k_2$ integrals in Eq.(2.48) may be immediately performed, leaving

$$B_{\alpha,\beta} = \frac{2\pi q^4 n_\alpha n_\beta}{|\boldsymbol{v}\times\boldsymbol{v}'|}\ 2\int_{R>0}\mathrm{d}k \int_{-\infty}^{\infty}\mathrm{d}\omega\,\frac{\delta(\epsilon_{\mathrm{r}}(\boldsymbol{k},\omega))}{R^2|\mathrm{Im}\,\epsilon|}. \tag{2.49}$$

We remind the reader that this is the piece of $B_{\alpha,\beta}$ associated with field particle speeds or fluctuation phase speeds $v' \sim \omega/k \ll v_{Te}$ for which the collective enhancement is negligible and *total* $J(\boldsymbol{v})$ is, of course, the *sum* of both these contributions. Now, the dielectric function for ion acoustic waves

is

$$\mathrm{Re}\,\epsilon(k,\omega) = 1 - \frac{\omega_{\mathrm{p}i}^2}{\omega^2} + \frac{1}{k^2\lambda_{\mathrm{D}}^2}. \tag{2.50a}$$

$$\mathrm{Im}\,\epsilon(k,\omega) = \sqrt{\frac{\pi}{2}}\frac{\omega}{k^3}\left(\frac{1}{\lambda_{\mathrm{De}}^2 v_{Te}} + \frac{1}{\lambda_{\mathrm{Di}}^2 v_{Ti}} e^{-\omega^2/2k^2v_{Ti}^2}\right). \tag{2.50b}$$

Here λ_{De} and λ_{Di} are the electron and ion Debye lengths, respectively. Anticipating the result that

$$\omega^2 = \frac{k^2 c_{\mathrm{s}}^2}{1 + k^2\lambda_{\mathrm{De}}^2}$$

for ion acoustic waves, Eq.(2.50a, 2.50b) togother suggest that the strongest collective enhancement will come from short wavelength (i.e. $k^2\lambda_{\mathrm{De}}^2 \gtrapprox 1$), because $\mathrm{Im}\,\epsilon(k,\omega)$ is smaller for these scales, since

$$\mathrm{Im}\,\epsilon(k,\omega) \sim \frac{1}{k^2\lambda_{\mathrm{De}}^2}\frac{\omega}{kv_{Te}}.$$

For such short wavelengths, then

$$\begin{aligned}\delta(\epsilon_{\mathrm{r}}) &\cong \delta(1 - \omega_{\mathrm{p}i}^2/\omega^2) \\ &= \frac{1}{2}\omega_{\mathrm{p}i}\big[\delta(\omega - \omega_{\mathrm{p}i}) + \delta(\omega + \omega_{\mathrm{p}i})\big].\end{aligned}$$

Evaluating $B_{\alpha,\beta}$, as given by Eqs. (2.48) and (2.49), in this limit then finally gives,

$$\begin{aligned}B_{\alpha,\beta} &= \left(\frac{4\pi q^2\omega_{\mathrm{p}i}n_\alpha n_\beta}{|\boldsymbol{v}\times\boldsymbol{v}'|}\right)\int\frac{\mathrm{d}k}{k^2|\mathrm{Im}\,\epsilon(k,\omega_{\mathrm{p}i})|} \\ &= \frac{2\sqrt{2\pi}q^4 v_{T_e}\lambda_{\mathrm{D}_e}^2}{|\boldsymbol{v}\times\boldsymbol{v}'|\lambda_{\mathrm{D}_i}^2}n_\alpha n_\beta\int\mathrm{d}\xi\Big/\left[1+\exp\left(-\frac{1}{2\xi}+\frac{L}{2}\right)\right],\end{aligned} \tag{2.51a}$$

where:

$$L = \ln\left[\left(\frac{T_e}{T_i}\right)^2\frac{m_i}{m_e}\right] \tag{2.51b}$$

and $\xi = k^2\lambda_{\mathrm{De}}^2$. Equation (2.51a) quite clearly illustrates that maximal relaxation occurs for *minimal* $\mathrm{Im}\,\epsilon(\xi,L)$, that is when $\exp[-1/2\xi + L/2] \ll$

1. That is, the collective enhancement of discreteness-induced scattering is determined by $\mathrm{Im}\,\epsilon$ for the least damped mode. This occurs when $\xi \lessapprox 1/L$, so that the dominant contribution to $B_{\alpha,\beta}$ comes from scales for which

$$k^2 = (\boldsymbol{k} \cdot \hat{n})^2 < 1/(\lambda_{\mathrm{De}}^2 L).$$

Note that depending on the values of L and the Coulomb logarithm ($\ln \Lambda$, which appears in the standard Coulombic scattering contribution to $B_{\alpha,\beta}$ from $v' \sim v_{Te}$), the collectively enhanced $B_{\alpha,\beta}$ due to low velocity field particles ($v' \ll v_{Te}$) may even exceed its familiar Coulomb scattering counterpart. Clearly, this is possible only when $T_e/T_i \gg 1$, yet not so large as to violate the tenets of the TPM and B-L theories.

2.2.4 Test Particle Model: Looking Back and Looking Ahead

In this section of the introductory chapter, we have presented the test particle model for fluctuations and transport near thermal equilibrium. As we mentioned at the beginning of the chapter, the TPM is the most basic and most successful fluctuation theory for weakly collisional plasmas. So, despite its limitation to stable, quiescent plasmas, the TPM has served as a basic paradigm for treatments of the far more difficult problems of *non-equilibrium* plasma kinetics, such as plasma turbulence, turbulent transport, self-organization etc. Given this state of affairs, we deem it instructive to review the essential elements of the TPM and place the subsequent chapters of this book in the context of the TPM and its elements. In this way, we hope to provide the reader with a framework from which to approach the complex and sometimes bewildering subject of the physical kinetics of non-equilibrium plasmas. The discussion which follows is summarized in Table 2.3. We discuss and compare the test particle model to its non-

equilibrium descendents in terms of both physics concepts and theoretical constructs.

Regarding *physics concepts*, the TPM is fundamentally a "near equilibrium" theory, which presumes a balance of emission and absorption at each k. In a turbulent plasma, non-linear interaction produces spectral transfer and a spectral cascade, which de-localize the location of absorption from the region of emission in $\boldsymbol{k}, \omega$ space. A spectral transfer turbulence energy from one region (i.e. emission) to another (i.e. damping). There two cases are contrasted in Fig.2.1.

A second key concept in the TPM is that emission occurs *only* via Cerenkov radiation from discrete test particles. Thus, since the only source for collective modes is discreteness, we always have

$$\boldsymbol{\nabla} \cdot \boldsymbol{\epsilon} E = 4\pi q \delta(\boldsymbol{x} - \boldsymbol{x}(t))$$

so

$$\left\langle \phi^2 \right\rangle_{\mathbf{k},\omega} = \frac{\left\langle \tilde{n}^2 \right\rangle}{|\epsilon(\mathbf{k},\omega)|^2}.$$

In contrast, for non-equilibrium plasmas, nonlinear coupling produces incoherent emission so the energy in mode $\boldsymbol{k}$ evolves according to

$$\frac{\partial}{\partial t}\left\langle E^2 \right\rangle_{\boldsymbol{k}} + \left(\sum_{\boldsymbol{k}'} C(\boldsymbol{k},\boldsymbol{k}') \left\langle E^2 \right\rangle_{\boldsymbol{k}'} \mathcal{T}_{c_{\boldsymbol{k},\boldsymbol{k}'}} \right) \left\langle E^2 \right\rangle_{\boldsymbol{k}} + \gamma_{\mathrm{d}\boldsymbol{k}} \left\langle E^2 \right\rangle_{\boldsymbol{k}}$$
$$= \sum_{\substack{\boldsymbol{p},\boldsymbol{q} \\ \boldsymbol{p}+\boldsymbol{q}=\boldsymbol{k}}} C(\boldsymbol{p},\boldsymbol{q}) \tau_{c\ \boldsymbol{p},\boldsymbol{q}} \left\langle E^2 \right\rangle_{\boldsymbol{p}} \left\langle E^2 \right\rangle_{\boldsymbol{q}} + S_{\mathrm{D}\boldsymbol{k}} \left\langle E^2 \right\rangle_{\boldsymbol{k}} \quad (2.52)$$

where $S_{\mathrm{D}\boldsymbol{k}}$ is the discreteness source and $\gamma_{\mathrm{d}\boldsymbol{k}}$ is the linear damping for the mode $\boldsymbol{k}$. For sufficient fluctuation levels, the nonlinear noise term (i.e. the first on the RHS) will clearly dominate over discreteness. A similar comment can be made in the context of the LHS of Eq.(2.52), written above. Nonlinear

Table 2.3. *Test particle model and its non-equilibrium descendents: physical concepts and theoretical constructs*

Test Particle Model	Non-Equilibrium Descendent
Physics Concepts	
emission vs. absorption balance per $\boldsymbol{k}$	spectral cascade, transfer, inertial range (Chapter 5, 6)
discreteness noise	incoherent mode-coupling (Chapter 5, 6), granulation emission (Chapter 8)
relaxation by screened collisions	collective instability driven relaxation, quasilinear theory, granulation interaction (Chapter 3, 8)
Theoretical Constructs	
linear response unperturbed orbit	turbulence response, turbulent diffusion, resonance broadening (Chapter 4,6)
damped mode response	nonlinear dielectric, wave-wave interaction, wave kinetics (Chapter 5, 6)
mean field theory	mean field theory without and with granulations (Chapter 3, 8)
discreteness-driven stationary spectrum	wave kinetics, renormalized mode coupling, disparate scale interaction (Chapter 5 - 7)
Balescu-Lenard, screened Landau equations	quasilinear theory granulation relaxation theory (Chapter 3, 8)

damping will similarly eclipse linear response damping for sufficiently large fluctuation levels.

A third physics concept is concerned with the mechanism physics of relaxation and transport. In the TPM, these occur only via screened collisions.

Collective effects associated with weakly damped modes may enhance relaxation but do not fundamentally change this picture. In a non-equilibrium plasma, collective modes can drive relaxation of the unstable $\langle f \rangle$, and nonlinear transfer can couple the relaxation process to thus enhance its rate.

In the realm of *theoretical constructs* and methods, *both* the test particle model and its non-equilibrium counterparts are fundamentally mean-field type approaches. However, they differ dramatically with respect to particle and model responses, nature of the wave spectrum and in how relaxation is calculated. The TPM assumes linear response theory is valid, so particle response functions exhibit only 'bare' Landau resonances. In contrast, scattering by strong electric field fluctuations will *broaden* the Landau resonance and *renormalize* the Landau propagator, so that,

$$\begin{aligned} R_{k,\omega} &\sim e^{ikx} \int_0^\infty e^{i\omega\tau} e^{-ikx(-\tau)} \mathrm{d}\tau \\ &\sim \int_0^\infty e^{i(\omega - kv)\tau} \mathrm{d}\tau = i/(\omega - kv) \end{aligned} \tag{2.53a}$$

becomes

$$\begin{aligned} R_{k,\omega} &\sim \int_0^\infty e^{i\omega\tau}\ e^{-ikx_0(-\tau)} \left\langle e^{-ik\delta x(-\tau)} \right\rangle \mathrm{d}\tau \\ &\sim \int_0^\infty e^{i(\omega - kv)\tau - \frac{k^2 D}{3}\tau^3} \mathrm{d}\tau \sim i/(\omega - kv + i/\tau_c), \end{aligned} \tag{2.53b}$$

where $1/\tau_c = (k^2 D/3)^{1/3}$. This is equivalent to the renormalization

$$\big[-i(\omega - kv) \big]^{-1} \rightarrow \left[-i(\omega - kv) - \frac{\partial}{\partial v} D \frac{\partial}{\partial v} \right]^{-1}. \tag{2.53c}$$

Here $D = D[\langle E^2 \rangle]$ is a functional of the turbulence spectrum. In a similar way to that sketched in Eq. (2.53), collective responses are renormalized and broadened by nonlinear wave interaction. Moreover, in the non-equilibrium case, a separate wave kinetic equation for $N(k, \boldsymbol{x}, t)$, the wave population density, is required to evolve the wave population in the presence of sources,

non-linear interaction and refraction, etc. by disparate scales. This wave kinetic equation is usually written in the form

$$\frac{\partial N}{\partial t} + (\boldsymbol{v}_{\rm g} + \boldsymbol{v}) \cdot \boldsymbol{\nabla} N - \frac{\partial}{\partial \boldsymbol{x}}(\omega + \boldsymbol{k} \cdot \boldsymbol{v}) \cdot \frac{\partial N}{\partial \boldsymbol{k}} = S_{\boldsymbol{k}} N + C_{\boldsymbol{K}}(N). \qquad (2.54)$$

Since in practical problems, the mean field or coarse grained wave population density $\langle N \rangle$ is of primary interest, a similar arsenal of quasi-linear type closure techniques has been developed for the purpose of extracting $\langle N \rangle$ from the wave kinetic equation. We conclude by noting that this discussion, which began with the TPM, comes full circle when one considers the effect of nonlinear mode coupling on processes of relaxation and transport. In particular, mode localized coupling produces phase space density vortexes or eddys in the phase space fluid. These phase space eddys are called *granulations*, and resemble a macroparticle. Such granulations are associated with peaks in the phase space density correlation function. Since these granulations resemble macroparticles, it should not be too surprising that they drive relaxation via a mechanism similar to that of dressed test particles. Hence, the mean field equation for $\langle f \rangle$ in the presence of granulations has the *structure* of a Balescu-Lenard equation, though of course its components differ from those discussed in this chapter.

2.3 K41 Beyond Dimensional Analysis - Revisiting the Theory of Hydrodynamic Turbulence

We now turn to our second paradigm, namely Navier-Stokes turbulence, and the famous Kolmogorov cascade through the inertial range. This is *the* classic example of a system with dynamics controlled by a self-similar spectral flux. It constitutes the ideal complement to the TPM, in that it features the role of transfer, rather than emission and absorption. We also

discuss related issues in particle dispersion, two-dimensional turbulence and turbulent pipe flows.

2.3.1 Key Elements in Kolmogorov Theory of Cascade

2.3.1.1 Kolmogorov theory

Surely everyone has encountered the basic ideas of Kolmogorov's theory of high Reynolds number turbulence! Loosely put, empirically motivated assumptions of

i) spatial homogeneity - i.e. the turbulence is uniformly distributed in space,

ii) isotropy - i.e. the turbulence exhibits no preferred spatial orientation,

iii) self-similarity - i.e. all inertial range scales exhibit the same physics and are equivalent. Here "inertial range" refers to the range of scales ℓ smaller than the stirring scale ℓ_0 but larger than the dissipation scale ($\ell_d < \ell < \ell_0$),

iv) locality of interaction - i.e. the (dominant) nonlinear interactions in the inertial range are local in scale, i.e. while large scales advect small scales, they cannot distort or destroy small scales, only sweep them around. Inertial range transfer occurs via like-scale straining, *only*.

Assumptions i) - iv) and the basic idea of an inertial range cascade are summarized in Fig.2.12. Using assumptions i) - iv), we can state that energy thru-put must be constant for all inertial range scales, so

$$\epsilon \sim v_0^3/\ell_0 \sim v(\ell)^3/\ell, \tag{2.55a}$$

and

$$v(\ell) \sim (\epsilon\ell)^{1/3}, \tag{2.55b}$$

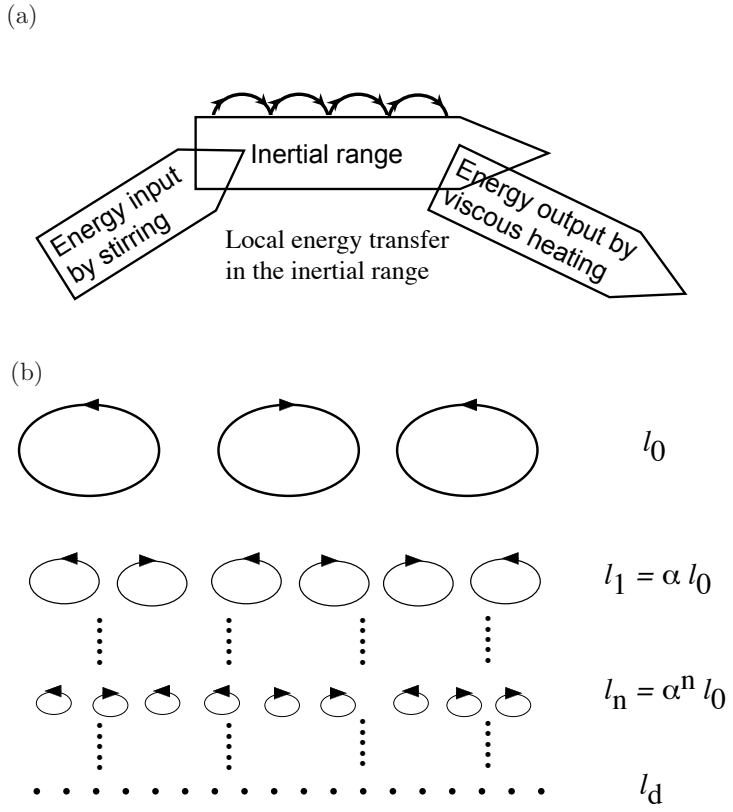

Fig. 2.12. Basic cartoon explanation of the Richardson-Kolmogorov cascade. Energy transfer in Fourier-space (a), and real space (b).

$$E(k) \sim \epsilon^{2/3} k^{-5/3}, \tag{2.55c}$$

which are the familiar K41 results. The dissipation scale ℓ_d is obtained by balancing the eddy straining rate $\epsilon^{1/3}/\ell^{2/3}$ with the viscous dissipation rate ν/ℓ^2 to find the Kolmogorov microscale,

$$\ell_d \sim \nu^{3/4}/\epsilon^{1/4}. \tag{2.56}$$

2.3.1.2 Richardson theory of particle separation

A related and important phenomenon, which also may be illuminated by scaling arguments, is how the distance between two test particles grows in time in a turbulent flow. This problem was first considered by Louis Fry Richardson, who was stimulated by observations of the rate at which pairs of weather balloons drifted apart from one another in the (turbulent) atmosphere. Consistent with the assumption of locality of interaction in scale, Richardson ansatzed that the distance between two points in a turbulent flow increases at the speed set by the eddy velocity on scales corresponding (and comparable) to the distance of separation (Fig. 2.13). Thus, for distance ℓ,

$$\frac{d\ell}{dt} = v(\ell), \tag{2.57a}$$

so using the K41 results (2.55b) gives

$$\ell(t) \sim \epsilon^{1/3} t^{3/2}, \tag{2.57b}$$

a result which Richardson found to be in good agreement with observations. Notice that the distance of separation grows *super-diffusively*, i.e. $\ell(t) \sim t^{3/2}$, and not $\sim t^{1/2}$, as in the textbook case of Brownian motion. The super-diffusive character of $\ell(t)$ is due to the fact that larger eddys support larger speeds, so the separation process is *self-accelerating*. Note too, that the separation grows as a power of time, and not exponentially, as in the case of a dynamical system with positive Lyapunov exponent. This is because for each separation scale ℓ, there is a *unique* corresponding separation velocity $v(\ell)$, so in fact there is a *continuum* of Lyapunov exponents (one for each scale) in the case of a turbulent flow. Thus, $\ell(t)$ is algebraic, not exponential! By way of contrast, the exponential rate of particle pair

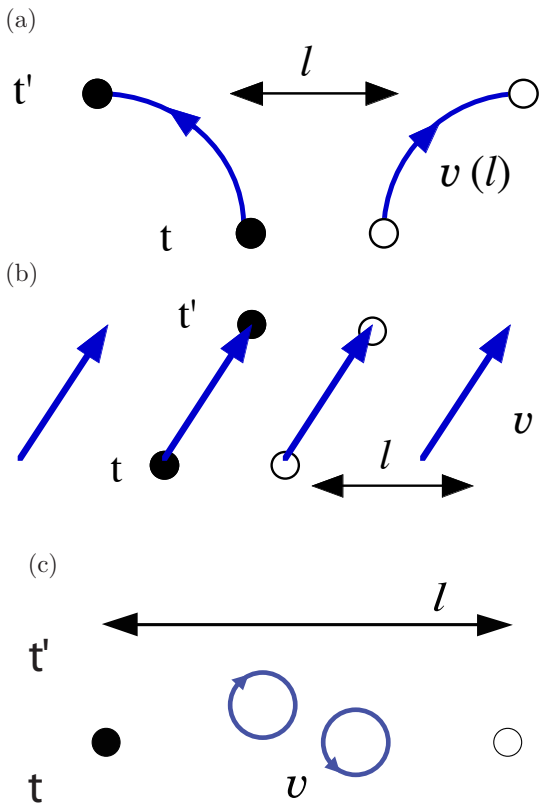

Fig. 2.13. Basic idea of the Richardson dispersion problem. The evolution of the separation of the two points (black and white dots) l follows the relation $dl/dt = v$ (a). If the advection field scale exceeds l, the particle pair swept together, so l is unchanged (b). If the advection field scale is less than l, there is no effect (except diffusion) on particle dispersion (c).

separation in a smooth chaotic flow is set by the largest positive Lyapunov exponent. We also remark here that while intermittency corrections to the K41 theory based upon the notion of a dissipative attractor with a fractal dimension less than three have been extensively discussed in the literature, the effects of intermittency in the corresponding Richardson problem have received relatively little attention. This is unfortunate, since, though it may

seem heretical to say so, the Richardson problem is, in many ways, more fundamental than the Kolmogorov problem, since unphysical effects due to sweeping by large scales are eliminated by definition in the Richardson problem. Moreover, the Richardson problem is of interest to calculating the rate of turbulent dispersion and the lifetime of particles or quasiparticles of turbulent fluid. An exception to the lack of advanced discussion of the Richardson problem is the excellent review article by Falkovich, Gawedski and Vergassola, 2001.

2.3.1.3 Stretching and generation of enstrophy

Of course, 'truth in advertising' compels us to emphasize that the scaling arguments presented here contain no more physics than that which was inserted ab initio. To understand the *physical mechanism* underpinning the Kolmogorov energy cascade, one must consider the dynamics of structures in the flow. As is well known, the key mechanism in 3D Navier-Stokes turbulence is *vortex tube stretching*, schematically shown in Fig. 2.14. There, we see that alignment of strain $\boldsymbol{\nabla v}$ with vorticity $\boldsymbol{\omega}$ (i.e. $\boldsymbol{\omega} \cdot \boldsymbol{\nabla v} \neq 0$) *generates* small scale vorticity, as dictated by angular momentum conservation in incompressible flows. The enstrophy (mean squared vorticity) thus diverges as

$$\langle \omega^2 \rangle \sim \epsilon / \nu, \tag{2.58}$$

for $\nu \to 0$. This indicates that *enstrophy is produced in 3D turbulence*, and suggests that there may be a *finite time singularity* in the system, an issue to which we shall return later. By finite time singularity of enstrophy, we mean that the enstrophy diverges within a finite time (i.e. with a growth rate which is faster than exponential). In a related vein, we note that finiteness of ϵ as $\nu \to 0$ constitutes what is called an *anomaly* in quantum field theory.

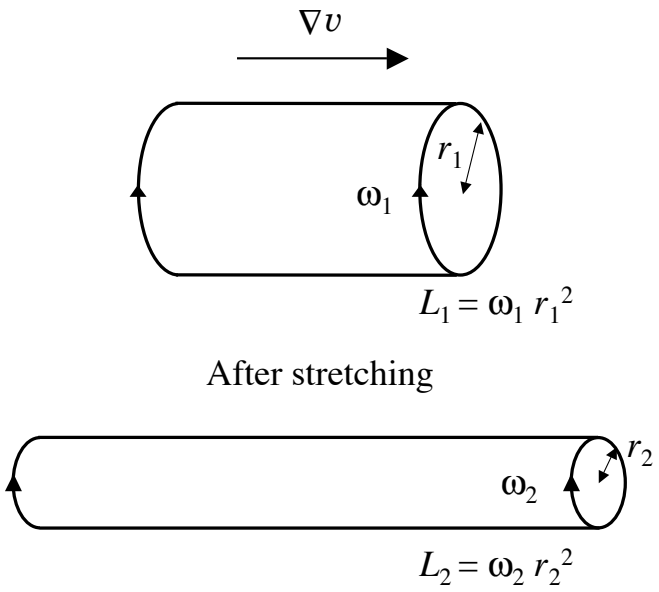

Fig. 2.14. The mechanism of enstrophy generation by vortex tube stretching. The vortex tube stretching vigorously produces small scale vorticity.

An anomaly occurs when symmetry breaking (in this case, breaking of time reversal symmetry by viscous dissipation) persists as the symmetry breaking term in the field equation asymptotes to zero. The scaling $\langle \omega^2 \rangle \sim 1/\nu$ is suggestive of an anomaly. So is the familiar simple argument using the Euler vorticity equation (for $\nu \to 0$)

$$\frac{d\boldsymbol{\omega}}{dt} = \boldsymbol{\omega} \cdot \boldsymbol{\nabla} \boldsymbol{v}, \tag{2.59a}$$

$$\frac{d}{dt}\omega^2 \sim \omega^3. \tag{2.59b}$$

Of course, this "simple argument" is grossly over-simplified, and incorrect.† In two dimensions $\boldsymbol{\omega} \cdot \boldsymbol{\nabla v} = 0$, so enstrophy is conserved. As first shown by Kraichnan, this necessitates a *dual cascade*, in which enstrophy *forward cascades* to small scales, while energy *inverse cascades* to large scales. The mechanism by which the dual conservation of energy and enstrophy force a dual cascade in 2D turbulence is discussed further later in this chapter.

2.3.1.4 Fundamental hypothesis for K41 theory

As elegantly and concisely discussed by U. Frisch in his superb monograph "Turbulence - The Legacy of A.N. Kolmogorov", the K41 theory can be systematically developed from a few fundamental hypotheses or postulates. Upon proceeding, the cynical reader will no doubt conclude that the hypotheses H1)-H4) stated below are simply restatements of assumptions i)-iv). While it is difficult to refute such a statement, we remark here that H1)-H4), *are* indeed of value, both for their precise presentation of Kolmogorov's deep understanding and for the insights into his thinking which they provide. As these postulates involve concepts of great relevance to other applications, we revisit them here in preparation for our subsequent discussions. The first fundamental hypotheses of the K41 theory is:

H1) As Reynolds number $R_e \to \infty$, all possible symmetries of the Navier-Stokes equation, usually broken by the means of turbulence initiation or production, are restored in a statistical sense at small scales, and away from boundaries.

† In fact, a mathematical proof of finite time singularity of enstrophy remains an elusive goal, with an as-yet-unclaimed Clay prize of $1,000,000. (2007)

The reader should note that H1) is a deceptively simple, and fundamentally quite profound hypothesis! The onset or production of turbulence nearly always involves symmetry breaking. Some examples are:

i) shear flow turbulence: the initial Kelvin-Helmholtz instability results from breaking of translation and rotation symmetry.
ii) turbulence in a pipe with a rough boundary: the driving pressure drop, the wall and roughenings break symmetry.
iii) turbulence in a flushing toilet: the flow has finite chirality and is non-stationary.

Naively, one might expect the turbulent state to have some memory of this broken symmetry. Indeed, the essence of β-model and multi-fractal theories of intermittency is the persistence of some memory of the large, stirring scales into the smallest inertial range scales. Yet, the universal character of K41 turbulence follows directly from, and implies a restoration of, initially broken symmetry at small scales. Assumptions i) and ii) really follow from hypothesis H1).

The second K41 hypothesis is:

H2) Under the assumptions of H1), the flow is self-similar at small scales and has a unique scaling exponent h, such that

$$\boldsymbol{v}(\boldsymbol{r}, \lambda\ell) = \lambda^h \boldsymbol{v}(\boldsymbol{r}, \ell).$$

Here, $\boldsymbol{v}(\boldsymbol{r}, \ell)$ refers to the velocity wavelet field at position $\boldsymbol{r}$ and scale ℓ. Clearly, H2) implies assumptions iii) and iv), concerning self-similarity and

locality of interaction.

Hypotheses H1) and H2) pertain to flow structure and scaling properties. Two additional postulates pertain to dynamics. These are:

H3) Given the assumptions of H1) and H2), turbulent flow has a finite, non-vanishing mean rate of dissipation per unit mass ϵ, as $\nu \to 0$,

and

H4) In the limit of high but finite R_e, all small-scale statistical properties are uniquely and universally determined by ϵ and ℓ.

Hypothesis H3) is tacitly equivalent to stating that an anomaly exists in K41 turbulence. Note that ϵ is independent of ν. However, notice also that ϵ, the "mean rate of dissipation per unit mass" is not related to physical, calculable quantities, and is left as a more-than-slightly ambiguous concept. Introduction of fluctuations (which relax the statement 'uniquely' in H4) in the local dissipation rate (which in reality are usually associated with localized dissipative structures such as strong vortex tubes) and of a statistical distribution of dissipation, leads down the path to intermittency modelling, a topic which is beyond the scope of this book. The reader is referred to Frisch '95, for an overview, and to seminal references such as Frisch, Sulem, Nelkin '78, She and Leveque '94, Falkovich, Gawedski and Vergassola, 2001, and others for an in depth discussion of intermittency modifications to the K41 theory. Finally, hypothesis H4) relates all statistics to ϵ and ℓ, the only two possible relevant parameters, given H1), H4).

2.3.2 Two Dimensional Fluid Turbulence

In this subsection, we briefly summarize certain key features of the theory of two-dimensional (2D) fluid turbulence. Our attention will focus upon the dual cascades of energy and enstrophy in 2D turbulence, the dispersion of particle pairs (i.e., the Richardson problem), and on the emergence of long lived coherent structures in turbulent 2D flow. Two-dimensional fluid dynamics has many features in common with those of magnetized plasmas, and so is of great interest to us. The 2D fluid turbulence is a critically important paradigm for plasma turbulence. The literature of 2D turbulence theory and experiment is vast, so here we survey only the most basic and fundamental elements of this interesting story.

2.3.2.1 Forward and inverse cascade

As we have already discussed, the defining feature of 2D fluid dynamics is the absence of vortex tube stretching (i.e., $\boldsymbol{\omega} \cdot \nabla \boldsymbol{v} = 0$). Thus, vorticity is conserved locally, up to viscous dissipation, i.e.,

$$\frac{\partial}{\partial t}\boldsymbol{\omega} + \boldsymbol{v} \cdot \boldsymbol{\nabla}\boldsymbol{\omega} - \nu\nabla^2\boldsymbol{\omega} = 0, \tag{2.60a}$$

or, representing $\boldsymbol{v}$ using a stream function, $\boldsymbol{v} = \nabla\phi \times \hat{z}$ (where $\hat{z}$ is the coordinate in the direction of uniformity) and:

$$\frac{\partial}{\partial t}\nabla^2\phi + \nabla\phi \times \hat{z} \ \cdot \nabla\nabla^2\phi - \nu\nabla^4\phi = 0. \tag{2.60b}$$

The local, inviscid conservation of the vorticity *underlies many of the similarities* between 2D fluid dynamics and Vlasov plasma dynamics. In particular, we note that the equation for an inviscid 2D fluid is just

$$\frac{d\rho}{dt} = 0$$

(for $\rho = \nabla^2\phi$) which is similar in structure of the Vlasov equation

$$\frac{df}{dt} = 0.$$

Both state that phase space density is conserved along particle orbits. Hence, from Eq.(2.60b), it follows that in two dimensions both energy

$$E = \iint d^2x \frac{v^2}{2} = \iint d^2x \frac{1}{2}|\nabla\phi|^2$$

and enstrophy

$$\Omega = \iint d^2x \frac{\omega^2}{2} = \iint d^2x \frac{1}{2}|\nabla^2\phi|^2$$

together are quadratic inviscid invariants. The existence of *two* conserved quantities complicates the construction of the theory of turbulent cascade for 2D turbulence. As we shall show, the resolution of this quandary is a dual cascade: That is, for forcing at some intermediate scale with wave number k_f such that $k_{\min} < k_f < k_{\max}$, there is

i) a self-similar, local enstrophy flux from k_f toward viscous damping at high k. This is called the forward *enstrophy cascade*.

ii) a self-similar, local energy flux from k_f toward *low* k and *large scale*. This is called the *inverse energy cascade*.

Obviously, the forward and inverse cascades must have distinct spectral power law scalings. Also, we remark that energy and enstrophy are each transferred in *both* directions, toward high and low k. What distinguishes the two cascade ranges is that the directions for *self-similar* transfer differ.

The need for a dual cascade picture can easily be understood from the following simple argument. Consider some initial spectral energy $E(k, t = 0)$ distributed over a range as shown by a dotted line in Fig.2.15. This initial

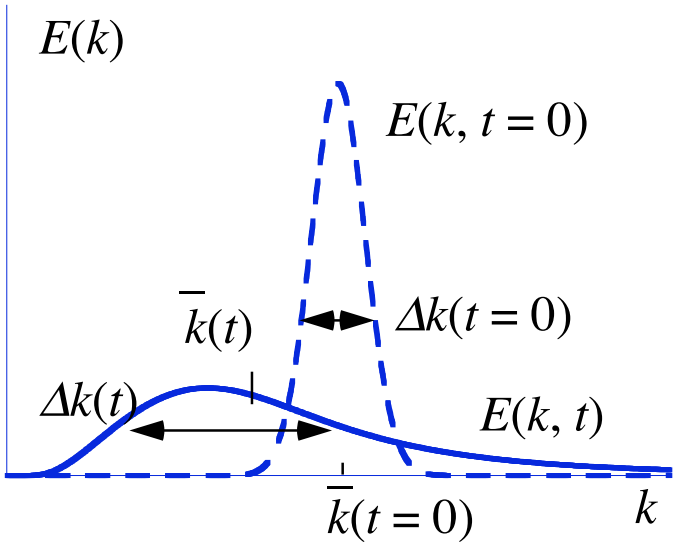

Fig. 2.15. Energy spectral density $E(k)$ shifts toward lower k (schematic illustration). As Δk^2increases, the centroid $\overline{k}$ decreases.

distribution has variance Δk^2 and centroid wave number $\overline{k}$

$$\Delta k^2 = \frac{1}{E}\int dk\big(k-\overline{k}\big)^2 E\,(k)\,, \tag{2.61a}$$

and

$$\overline{k} = \frac{1}{E}\int dk\; kE\,(k)\,. \tag{2.61b}$$

Now, it is eminently plausible that the turbulence will act to broaden Δk^2 as the spectrum evolves in time. Thus, we expect that, as time increases, Δk^2 will grow,

$$\frac{\partial}{\partial t}\Delta k^2 > 0. \tag{2.62}$$

However, we know that the relation $\int dk\big(k-\overline{k}\big)^2 E\,(k) = \Omega - \big(\overline{k}\big)^2 E$ holds and that Ω and E are (inviscidly) conserved, i.e.,

$$\Delta k^2 = \frac{\Omega\,(t=0)}{E\,(t=0)} - \big(\overline{k}\big)^2. \tag{2.63a}$$

Since $\Omega\big(t=0\big)/E\big(t=0\big)$ is constant, we see that the growth of Δk^2 (Eq.(2.62)) requires

$$\frac{\partial}{\partial t}\overline{k} < 0, \tag{2.63b}$$

so that the centroid of the spectrum must shift toward *lower* wave numbers. This is shown in Fig.2.15. This trend is quite suggestive of the *inverse* energy cascade.

We now repeat this type of exercise for the case of enstrophy. Here, it is convenient to work with *scale*, not wave number. Thus, for $l = 1/k$, we can define the variance

$$\Delta l^2 = \frac{1}{\Omega}\int dl\big(l-\bar{l}\big)^2\Omega\left(l\right), \tag{2.64a}$$

where $\Omega\left(l\right)$ is the enstrophy density and the total enstrophy is given by $\Omega = \int dl\Omega\left(l\right)$, and $\bar{l}$ is the enstrophy centroid scale

$$\bar{l} = \frac{1}{\Omega}\int dl\ l\Omega\left(l\right). \tag{2.64b}$$

Note that convergence of the moments of $\Omega\left(l\right)$ is assumed *a priori*, but *not* proved. Then the change of the variance is given as

$$\frac{\partial}{\partial t}\Delta l^2 = \frac{\partial}{\partial t}\left\{\frac{1}{\Omega}\int dl\big(l-\bar{l}\big)^2\Omega\left(l\right)\right\} = \frac{\partial}{\partial t}\left\{\frac{1}{\Omega}\int dl\ l^2\Omega\left(l\right) - \big(\bar{l}\big)^2\right\}. \tag{2.65a}$$

However, the integral $\int dll^2\Omega\left(l\right)$ is just the total energy, which is conserved along with the total enstrophy. Hence,

$$\frac{\partial}{\partial t}\Delta l^2 = -\frac{\partial}{\partial t}\big(\bar{l}\big)^2. \tag{2.65b}$$

For the range of scales to broaden in time (i.e., $\partial\Delta l^2/\partial t > 0$),

$$\frac{\partial}{\partial t}\bar{l} < 0 \tag{2.66}$$

is required, so the centroid of the distribution of enstrophy density (by scale) must move toward *smaller* scale. This is suggestive of a direct cascade of

enstrophy to smaller scale. Thus, we see that the simultaneous conditions of spectral broadening and inviscid conservation of energy and enstrophy force the dual cascade model. In this dual cascade scenario, enstrophy is self-similarly transferred to smaller scales while energy is self-similarly transferred to large scales.

2.3.2.2 Self-similar spectral distribution

Simple scaling arguments for the cascade spectra are then easily to construct. To describe the cascade spectra, it is convenient to work with the energy density spectrum $E(k)$, so with a factor of k for density of states, $kE(k)$ has the dimension of $\langle v^2 \rangle$. Hence $k^3 E(k)$ corresponds to enstrophy density. Spectral self-similarity leads us to hypothesis that enstrophy cascades locally, with a rate set by the eddy-turn-over time τ_{et} for each k, i.e.,

$$\frac{1}{\tau_{cascade}} = \frac{1}{\tau_{\text{et}}} = \frac{v(l)}{l} = k(kE(k))^{1/2}. \tag{2.67}$$

Then, a scale-independent enstrophy dissipation rate $\eta = k^3 E(k) / \tau_{\text{cascade}}$ requires that

$$\left(k^3 E(k)\right)^{3/2} = \eta, \tag{2.68a}$$

which immediately gives the energy spectrum for the (forward) enstrophy cascade as

$$E(k) = \eta^{2/3} k^{-3}. \tag{2.68b}$$

Note that the eddy-turn-over rate in the enstrophy cascade range is constant in k from Eqs. (2.67) and (2.68b). The enstrophy spectrum is given by $\Omega(k) = k^2 E(k)$, so that the equi-partition holds for $k\Omega(k)$ according to Eq. (6.68b). The physics of the enstrophy cascade is successfully described by the cartoon in Fig.2.16. This shows that stretching of iso-contours of

vorticity by a turbulent flow necessarily generates smaller scale structure in these contours, thus producing a net increase in mean square vorticity gradient $\left\langle \left(\boldsymbol{\nabla}\nabla^2\phi\right)^2 \right\rangle$. The increase is what underlies the forward enstrophy cascade process. The cascade is ultimately terminated by viscous mixing. The forward cascade of enstrophy in k space is closely related to the homogenization (i.e., mixing and dissipation) of vorticity in configuration space, to be discussed later.

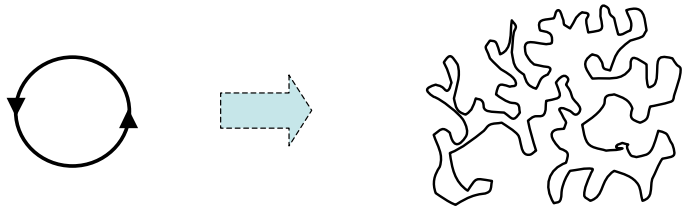

Fig. 2.16. Mean square vorticity increases as vorticity isocontours stretch in a turbulent flow.

The self-similar inverse cascade of energy is described correspondingly, by balancing the energy dissipation rate ε with the flow rate of energy to larger scale set locally by the eddy-turn-over rate, i.e., $kE\left(k\right)/\tau_{cascade} = \epsilon$. This gives the relation, with the help of Eq.(2.67)

$$k^{5/2}E\left(k\right)^{3/2} = \epsilon, \tag{2.69a}$$

so

$$E\left(k\right) = \epsilon^{2/3}k^{-5/3}. \tag{2.69b}$$

Of course, the energy cascade spectrum is the same as the K41 spectrum, though the cascade is toward large scale. For forcing at k_f, clearly here we

have

$$\epsilon k_f^2 = \eta.$$

The dual cascade is represented by the schematic drawing in Fig.2.17. Note that the inverse cascade builds up a large-scale flow from intermediate forcing. The process of large-scale build-up is nicely illustrated by Fig.2.18, which shows the evolution of the spectrum during a simulation of 2D turbulence forced at intermediate scale. Ultimately, this flow occupies the largest scale of the system, thus generating a macroscopic shear flow on that scale. The large-scale shears can then directly strain the smaller scales, thus breaching self-similarity and producing strong intermittency in the turbulent flow.

2.3.2.3 Dispersion of particle pairs

The dispersion of particle pairs (i.e. Richardson's problem) in a turbulent 2D flow is strongly tied to the dynamics of the dual cascades. In all cases, the dispersion of particles separated by distance l is determined by the eddies of that size, Eq.(2.57a), so

$$\frac{d}{dt} l = v\left(l\right).$$

For the inverse cascade range, i.e., $l > k_f^{-1}$, Eq.(2.69b) gives $v\left(l\right) = \varepsilon^{1/3} l^{1/3}$, so

$$l\left(t\right)^2 \sim \varepsilon\ t^3, \tag{2.70}$$

as in K41. Particle pairs grow super diffusively. For the forward, enstrophy cascade range, $l < k_f^{-1}$, we note that the velocity $v\left(l\right) = \left(kE\left(k\right)\right)^{1/2}$ is given by $\eta^{1/3} l$, because $E\left(k\right) = \eta^{2/3} k^{-3}$ holds as Eq.(2.68b). We immediately

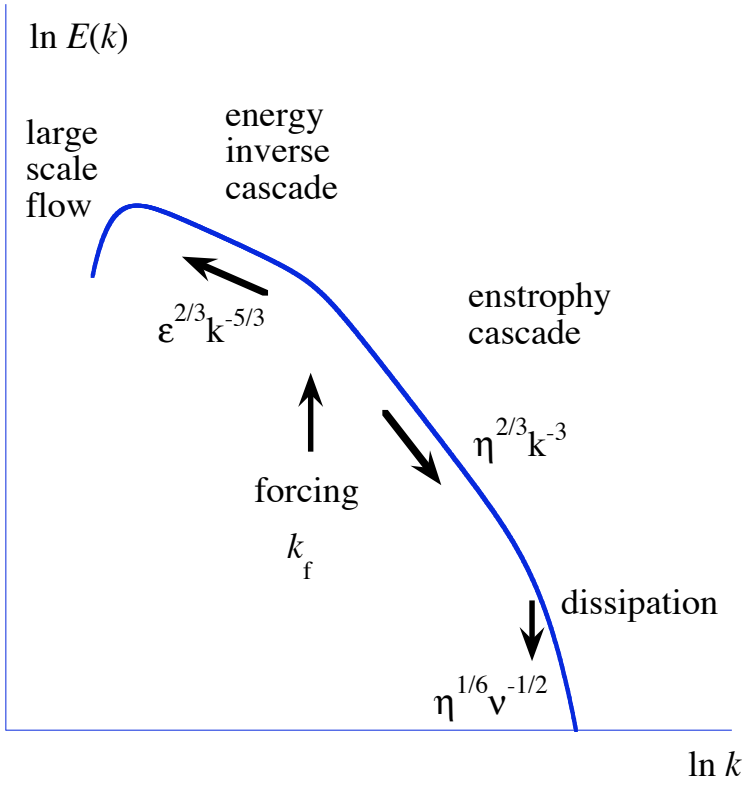

Fig. 2.17. Schematic of energy spectrum for dual cascade.

have

$$\frac{d}{dt}l = \eta^{1/3}l. \tag{2.71}$$

Thus, particle separation $l\,(t)$ grows exponentially in time for separation scales smaller than the forcing scale, but super diffusive growth for scales larger than the forcing scale. The exponential divergence of particles in the enstrophy cascade range resembles the exponential divergence of trajectories in a stochastic system, such as for the case of overlapping resonances between plasma particles and a spectrum of waves.

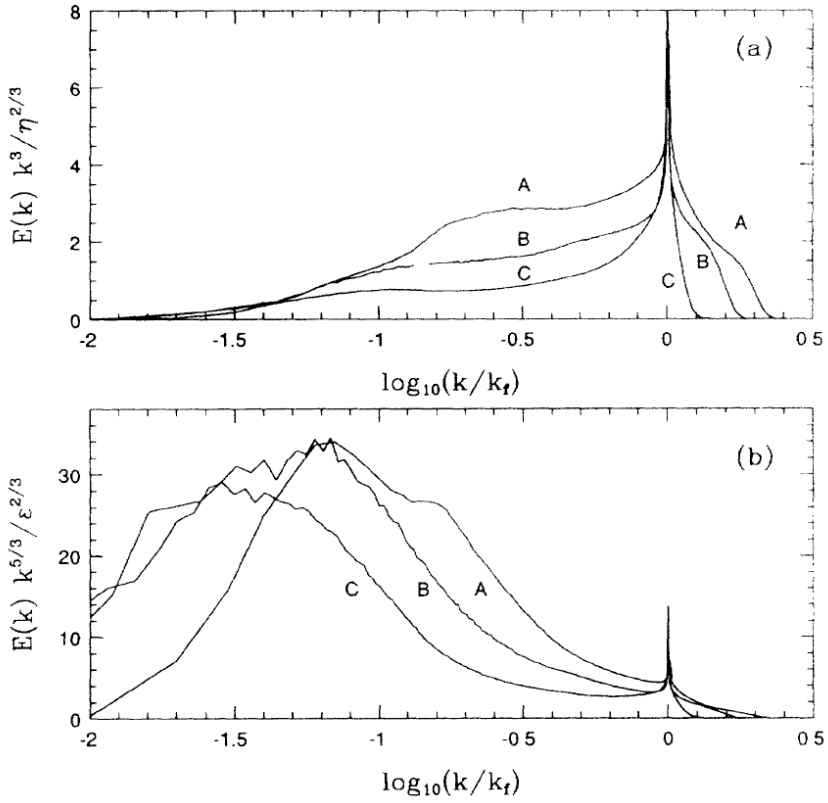

Fig. 2.18. Build-up of a large-scale flow in dual cascade [V. Borue, PRL **71** (1994) 1475]. Energy spectra normalized as (a) $E(k)\,k^3\eta^{-2/3}$ and (b) $E(k)\,k^{5/3}\varepsilon^{-2/3}$ as the function of $\log_{10}(k/k_f)$ for three different parameters in simulations. (B and C have finer resolution than A. In C, forcing occurs at finer scale than in B. See [Borue] for details of parameters.)

2.3.2.4 Long lived vortices

It is interesting to note that long-lived coherent vortices have been observed to emerge from decaying turbulent flows, and even in certain forced turbulent flows. This important phenomenon has long been observed, but was

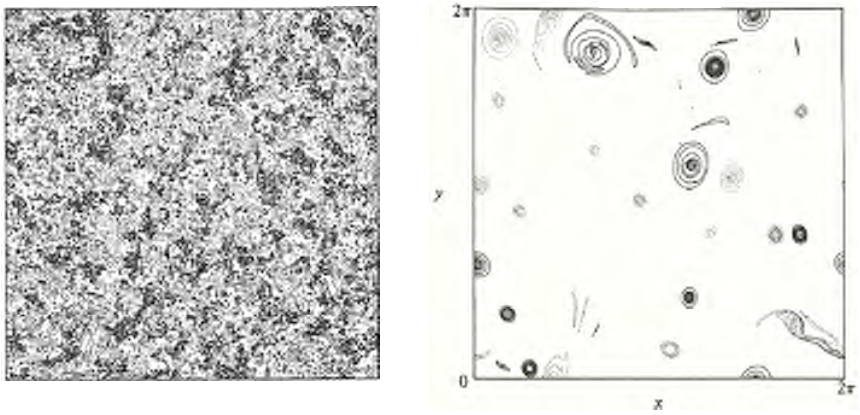

Fig. 2.19. Vorticity contours in the initial condition (a) and long-time evolution at a normalized time of $t = 16.5$ (b), where the eddy-turn-over time increases from 0.5 to 2.0 in the decay process. [J. C. McWilliams, JFM **146** (1984) 21]

dramatically emphasized by the seminal work of J. McWilliams and its offshoots. These studies revealed a two-stage evolution for decaying turbulence, namely:

i) a fast stage of rapid decay and cascading, as shown in Fig.2.19(a)

ii) a second, slower stage of evolution by binary vortex interaction. In this stage, vortices advect and strain each other, merge and sometimes form persisting pairs. Example of this evolution is shown in Fig.2.19(b).

One of the most interesting aspects of this work is that it confirms the intuitively appealing Okubo-Weiss criterion, which constitutes a plausible answer (for 2D fluids) to the often-asked question of "What makes a coherent structure coherent?"

The Okubo-Weiss criterion emerges from an asymptotic expression for the time evolution of the local vorticity gradient $\nabla\rho$ (where $\rho = \nabla^2\phi$ is the local

vorticity), which predicts that

$$\frac{\partial}{\partial t}\nabla\rho = \sqrt{S^2 - \rho^2}. \tag{2.72}$$

Here, $S = \partial^2\phi/\partial x\partial y$ is the local flow shear. The Okubo-Weiss (O-W) criterion thus states that the evolution of the local vorticity gradient is set by the Gaussian curvature of the stream function. In physical terms, the O-W criterion states that when the magnitude of the local shear exceeds the magnitude of local vorticity, the vorticity gradient is steeper and small scales will develop, as they do in enstrophy cascade. If the local enstrophy density exceeds $|S|$, however, the vorticity gradient will not steepen, and a coherent vortex will simply rotate, without distortion. Locally, the flow will be stable to the cascade process. The O-W criterion is quite plausible, as it is consistent with the expected natural competition between shearing and vortical circulation. Comparisons with simulations of decaying turbulence indicate that the O-W criterion successfully predicts the location of long lived, coherent vortices, which are, in some sense, stable to cascading, in a turbulent flow. Indeed, when applied to a fully turbulent flow, the O-W criterion successfully predicts the subsequent emergence and locations of coherent vortices after the early phase of rapid decay. Thus, the O-W criterion constitutes one physically plausible approach to predicting intermittency in 2D turbulence.

Here, intermittency refers to breakdown of self-similar transfer by the formation of stable structures. We should caution the reader that many types of intermittency are plausible. (For instance, another origin of intermittency, which is induced by the statistical variance of dissipation rate ε from its mean $\langle\epsilon\rangle$, is explained in [Yoshizawa, Arimitsu].) A full discussion of this challenging, forefront problem requires a book itself.

2.3.3 Turbulence in Pipe and Channel Flows

2.3.3.1 Illustration of problem

We now turn to the interesting and relevant problem of turbulence in pipe and channel flows, which we hereafter refer to simply as 'turbulent pipe flow'. The essence of the pipe flow problem is the calculation of the mean flow profile $V(y)$ for flow of a fluid with viscosity ν through a long pipe with fixed pressure drop per length $\Delta p/L$, assuming no-slip boundary conditions. The geometry and coordinates (after convention) are illustrated in Fig.2.20.

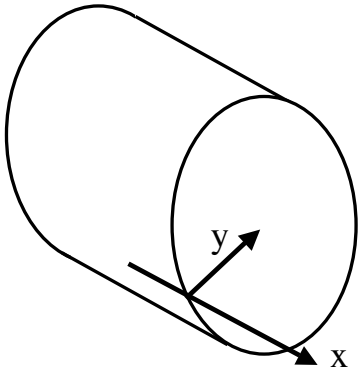

Fig. 2.20. Geometry of the pipe flow. The y-axis is measured from the wall (perpendicular to the wall) according to the convention.

As we shall see, there are many parallels between the K41 paradigm of homogeneous turbulence in a periodic box and the problem of turbulent flow in a pipe. The study of turbulent pipe flow was pioneered by Ludwig Prandtl in seminal works published in 1932 and 1945, hereafter referred to as P32, 45. The parallel between the K41 and P32, 35 problems is summarized in subsection 2.3.4.

Like K41 turbulence, pipe flow turbulence manifests an element of universality in its phenomenology. In simple terms, pipe flow turbulence is driven by turbulent mixing of the cross-stream shear of the mean flow $dV_x(y)/dy$ by turbulent Reynolds stress $\left\langle \tilde{V}_y \tilde{V}_x \right\rangle$, so that turbulent energy production P is given by:

$$P = -\left\langle \tilde{V}_y \tilde{V}_x \right\rangle \frac{d}{dy} V_x(y). \tag{2.73}$$

We therefore see that the turbulence is driven by the cross-stream flux of along stream momentum. Pipe flow is perhaps the simplest example of flux-driven turbulence, a ubiquitous paradigm with many applications to tokamaks, solar convection, etc.

The effective drag on the flow, which opposes the driving $\Delta p/L$, results from turbulent transport to the pipe wall, where the no-slip boundary condition forces the stream-wise flow to vanish. Thus, turbulent transport transfers or connects momentum input or drive by pressure drop to dissipation in the viscosity dominated region close to the no-slip boundary. A cartoon of this spatial transport process and its implications for the flow profile is given in Fig.2.21.

2.3.3.2 Viscous sublayer

The Reynolds stress $\left\langle \tilde{V}_y \tilde{V}_x \right\rangle$ is an effective measure of momentum transport to the wall, or equivalently, the stress exerted on the wall, which we call

$$T_{\mathrm{w}} = \rho \left\langle \tilde{V}_y \tilde{V}_x \right\rangle.$$

Here ρ indicates the mass density and T_{w} is the stress (not temperature). Clearly, T_{w} is proportional to $\Delta p/L$. Since there is no sink of momentum

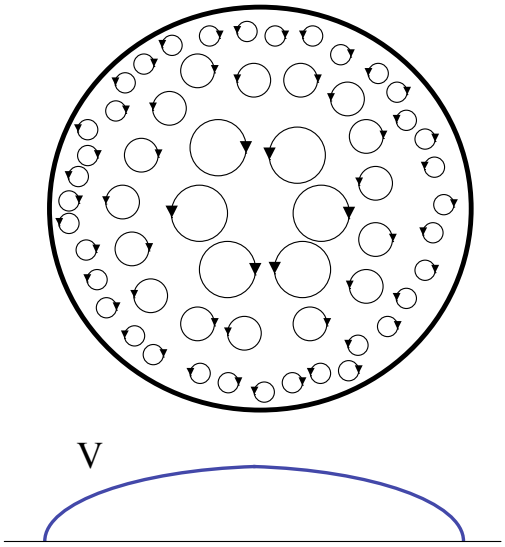

Fig. 2.21. Schematic drawings of the turbulent eddies in the cross-section of the pipe flow and the mean velocity profile across the mid plane.

other than viscous drag at the wall, the force balance on the fluid requires

$$T_{\rm w} = \frac{a}{2L}\Delta p.$$

For the turbulent stress near the wall, $T_{\rm w}$ is constant across the flow, and so we can define a constant friction velocity

$$V_* = \sqrt{T_{\rm w}/\rho},$$

where the mass density ρ is taken constant here for the transparency of the argument. V_* is a characteristic turbulent velocity for a pipe flow. (Note that the relation $V_* \propto \sqrt{\Delta p/\rho}$ holds.)

Having defined the characteristic velocity (which is called friction velocity) V_*, we can immediately identify two characteristic scales and Reynolds

numbers for pipe flow turbulence. One is the viscous sublayer width y_d,

$$y_d = \nu V_*^{-1}, \tag{2.74}$$

which is a measure of the thickness of the viscosity-dominated range near the wall. In the viscous sublayer, $y < y_d$, the Reynolds number $R_e = V_* y$ satisfies the relation $R_e < 1$. In order to balance the constant wall stress and satisfy the no-slip boundary condition at the wall, the flow profile must be linear, i.e., $V(y) \sim V_* y/y_d$, in the viscous sublayer. Of course, the flow further away from the wall is strongly turbulent, and the Reynolds number computed with the pipe cross-section length a, $R_e = V_* a/\nu$, is much larger than unity. Indeed, in practical applications, R_e is so large that all vestiges of the (subcritical) instability process, which initially triggered the turbulence, have been obliterated in the fully evolved turbulent state.

2.3.3.3 Log law of the wall

As with the K41 problem, empirical observation plays a key role in defining the problem. In the pipe flow problem, numerous experimental studies over a broad range of turbulent flows indicate that the flow profile has a universal, self-similar structure consisting of three layers, namely:

a) the core; i.e., $y \sim a$

b) an inertial sublayer; i.e., $y_d < y \ll a$

c) the viscous sublayer; i.e., $0 < y < y_d$,

and that in the inertial sublayer, the flow gradient is scale independent, with a universal structure of the form

$$\frac{d}{dy} V(y) \simeq \frac{V_*}{y}, \tag{2.75a}$$

so

$$V(y) = \kappa V_* \ln y. \tag{2.75b}$$

This logarithmic profile for the inertial sublayer flow is often referred to as the (Prandtl) Law of the Wall, and is, to reasonable accuracy, a universal feature of high R_e pipe flow. The flow profile and the three regimes are sketched in Fig.2.22. The empirically determined constant, $\kappa = 0.4$, is named the von Karman constant.

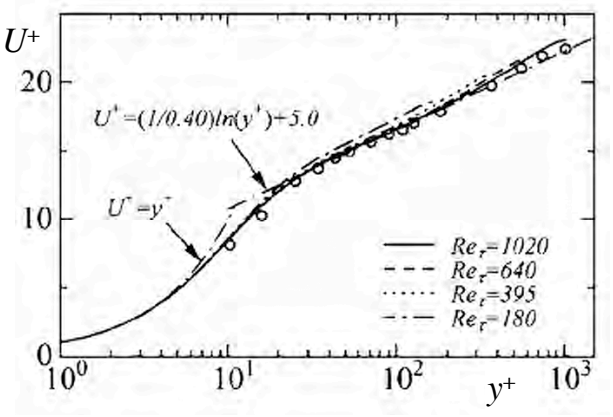

Fig. 2.22. Mean velocity of turbulent channel flows normalized by the friction velocity, $U^+ = V(y)/V_*$ as a function of the normalized distance $y^+ = y/y_d$. Quoted from [Yoshizawa et al. Physics of fluids **17**, 075113 (2005)], which compiled the lines, DNS [H. Abe, et al. Int. J. Heat Fluid Flow **25**, 404 (2004)] and circles, observation [T. Wei and W. W. Willmarth, J. Fluid Mech. **204**, 57 (1989)] at $R_{e\tau} = 1016$. Here, $R_{e\tau}$ is the Reynolds number defined by use of the friction velocity V_*. Viscous flow near wall, log law and core profile are observed.

We should mention here that though the logarithmic law of the wall profile is the best known feature of turbulent pipe flow, it is perhaps *more instructive to focus on the universality of the flow profile gradient* $dV(y)/dy$. Note

that the local gradient is determined entirely by the distance from the wall y (a purely local parameter!) and the friction velocity V_*. In same sense, it is more appropriate to focus on the flow gradient instead of flow, since the former is determined purely locally, while the flow at y is affected by physical effects originating at points far away.

A simple, physically appealing model can be constructed to explain the empirical law of the wall. The basic ideas of this model are:

i) turbulence intensity in the inertial sublayer is determined by a local balance between mean profile relaxation induced by turbulent viscosity $\nu_T$and turbulent dissipation of fluctuation energy,

ii) turbulence is characterized locally by a simple velocity, namely the friction velocity V_*, and a single length scale l.

Now, turbulence energy E evolves according to a competition between production P and dissipation ϵ, so

$$\frac{\partial}{\partial t}E = P - \epsilon, \tag{2.76a}$$

where

$$P = \nu_T \frac{\partial}{\partial y}V(y) = V_* l \frac{\partial}{\partial y}V(y), \tag{2.76b}$$

and

$$\epsilon = \frac{V_*^3}{l}. \tag{2.76c}$$

Here l is the characteristic length scale of the turbulence. Now, empirically we have $\partial V(y)/\partial y = V_*/y$, it follows that

$$\frac{\partial}{\partial t}E = V_* l \frac{V_*^2}{y^2} - \frac{V_*^3}{l}. \tag{2.76d}$$

Thus, we see that the most direct way to ensure stationality in the inertial sublayer is to simply take the characteristic length scale l to be y, the

distance from the wall,

$$l \sim y, \text{so } \nu_T = V_* y.$$

Note this ansatz ensures scale invariance in the inertial sublayer. The length $l \sim y$ is often referred to as the mixing length, since by analogy with gas kinetics where viscosity is given by thermal velocity and mean free path, $\nu = v_T l_{mfp}$, $l \sim y$ may be thought of as an effective mean free path, over which fluid momentum is mixed by a random walk with root-mean-square velocity V_*. In other words, the log law of the wall is based on the picture that the length of turbulent mixing l is given by the distance from the wall y (the upper bound by the vortex size in the region between the location y and the wall.).

This mixing length model of pipe flow turbulence was first proposed by Prandtl, and thus goes by the name of Prandtl Mixing Length Theory. Note that mixing length theory also immediately recovers the logarithmic profile, since by making the assumption of diffusive transport,

$$\frac{T_{\mathrm{w}}}{\rho} = \left\langle \tilde{V}_y \tilde{V}_x \right\rangle = \nu_T \frac{\partial}{\partial y} V(y), \tag{2.77a}$$

(note the minus sign is absorbed since y is measured from the wall) and if $\nu_T = V_* l = V_* y$, we have

$$\frac{\partial}{\partial y} V(y) = \frac{V_*}{y}. \tag{2.77b}$$

2.3.3.4 Approach of self-similarity

It is enlightening to briefly review another even simpler approach to the problem of the inertial sublayer profile, assuming similarity methods. To this end, one can formulate the problem by noting that since it is the *mean velocity gradient* which is locally determined self-similar and seemingly 'universal', we know that the dimensionless function $y V_*^{-1} \partial V(y) / \partial y$

is determined exclusively by the dimensionless parameters in the problem. Now, since there are two characteristic length scales in pipe flow turbulence, namely the viscous sublayer scale $y_d = \nu V_*^{-1}$ and pipe cross-section a, the relevant dimensionless function can be written as

$$\frac{y}{V_*}\frac{\partial V(y)}{\partial y} = F\left(\frac{y_d}{y}, \frac{y}{a}\right). \tag{2.78a}$$

For the inertial sublayer of a high Reynolds number pipe flow, $y/y_d \gg 1$ and $a/y \gg 1$. Thus, assuming complete Reynolds number similarity amounts to taking $y_d/y \to 0$ and $y/a \to 0$. In this limit,

$$\frac{y}{V_*}\frac{\partial V(y)}{\partial y} = F(0,0) \to const, \tag{2.78b}$$

so once again we arrive at the logarithmic Law of the Wall profile,

$$V(y) = \kappa V_* \ln y. \tag{2.78c}$$

Thus, we see that the Prandtl's law of the wall emerges from extremely simple arguments of complete Reynolds number similarity and scaling methods. The reader should note that study of corrections to the law of the wall induced by incomplete similarity is ongoing and remains an active topic of research.

2.3.4 Parallels between K41 and Prandtl's Theory

The parallel between the K41 and P32, 35 problems was referred many times during the discussion. At this point, the reader may wish to visit the summary in **Table 2.4**, to review the many parallels between the twin studies in self-similarity which constitute Kolmogorov's theory of the inertial range spectrum and Prandtl's theory of turbulent pipe flow. This table is largely self-explanatory. It is interesting, however, to comment on one place

where a parallel does not exist, namely, in the last entry, which deals with 'rigorous results'. For K41 theory, the '4/5 Law' is a rigorous asymptotic theorem which links the dissipation rate ϵ, the length scale l, and the triple moment $\left\langle \delta V^3 (l) \right\rangle$ by the relation

$$\left\langle \delta V^3 (l) \right\rangle = -\frac{4}{5}\epsilon l.$$

The 4/5 Law, derived from the Karman-Howarth relation, is perhaps the one true theorem, which is *proved* in turbulence theory. Since P32,45 theory tacitly assumes

$$\left\langle \delta V^3 (l) \right\rangle \underline{\simeq} V_*^3 \underline{\simeq} \epsilon y,$$

it is naturally desirable to know a theorem for turbulent pipe flow, which corresponds to the 4/5 law. Unfortunately, no such result is available at this time.

Table 2.4. *Parallel studies in self-similarity*

Inertial Range Spectrum (K41)	**Pipe Flow Profile (P32, 45)**
Basic ideas	
self-similarity in *scale*	self-similarity in *space*
inertial range spectrum $V(l)$	inertial sublayer profile $V(y)$
eddy/wavelet	mixing 'slug' or eddy
K41 spectrum	law of the wall
Range	
stirring	core
inertial	inertial sub-layer
dissipation	viscous sub-layer
Element	
$l \rightarrow$ eddy scale	$l_M = y \rightarrow$ mixing length
Through-put	
$\epsilon \rightarrow$ dissipation rate	$V_*^2 = T_W/\rho$
	$\rightarrow$ wall stress, friction velocity
Rate	
$1/\tau(l) \sim V(l)/l$ (eddy turn-over)	$\nu_T y^{-2} \sim V_*/y$ (ν_T : eddy viscosity)
Balance	
$\epsilon = V(l)^2/\tau(l)$	$V_*^2 \simeq \nu_T \partial V(y)/\partial y$
$V(l) \sim \epsilon^{1/3} l^{1/3}$	$\partial V(y)/\partial y \sim V_*/y \rightarrow$ long profile
Dissipation scale length	
$l_d = \nu^{3/4} \epsilon^{-1/4}$	$y_d = \nu V_*^{-1}$
Fit Constant	
Kolmogorov constant	von Karman constant
Theorem	
4/5 law	?